Facies distribution along salt walls: The Upper Cretaceous mixed siliciclastic-carbonate deposits of the Cotiella minibasins (Southern Pyrenees, Spain)

Kalifi Amir, Ribes Charlotte, Dietrich Pierre, Dujoncquoy Emmanuel, Muñoz Josep-Anton, Jean-Paul Callot, Ringenbach Jean-Claude

Journal Pre-proof

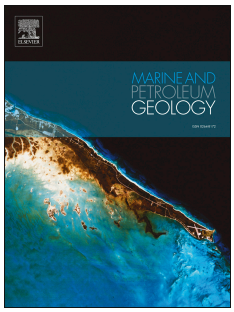

Facies distribution along salt walls: The Upper Cretaceous mixed siliciclastic-carbonate deposits of the Cotiella minibasins (Southern Pyrenees, Spain)

Kalifi Amir, Ribes Charlotte, Dietrich Pierre, Dujoncquoy Emmanuel, Muñoz Josep-Anton, Callot Jean-Paul, Ringenbach Jean-Claude

PII: S0264-8172(22)00467-6

DOI: https://doi.org/10.1016/j.marpetgeo.2022.105989

Reference: JMPG 105989

To appear in: *Marine and Petroleum Geology*

Received Date: 26 August 2022

Revised Date: 14 October 2022

Accepted Date: 18 October 2022

Please cite this article as: Amir, K., Charlotte, R., Pierre, D., Emmanuel, D., Josep-Anton, Muñ., Jean-Paul, C., Jean-Claude, R., Facies distribution along salt walls: The Upper Cretaceous mixed siliciclastic-carbonate deposits of the Cotiella minibasins (Southern Pyrenees, Spain), *Marine and Petroleum Geology* (2022), doi: https://doi.org/10.1016/j.marpetgeo.2022.105989.

Facies distribution along salt walls: the Upper Cretaceous mixed siliciclastic-carbonate deposits of the Cotiella minibasins (Southern Pyrenees, Spain)

Kalifi Amir[1, 2,], Ribes Charlotte[2], Dietrich Pierre[3], Dujoncquoy Emmanuel[2], Muñoz Josep-Anton[4], Callot Jean-Paul[1], Ringenbach Jean-Claude[2]*

Affiliations

1 : Laboratoire des fluides complexes et leurs réservoirs, LFCR, E2S-UPPA, CNRS, TotalEnergies Université de Pau et des Pays de l'Adour, avenue de l'Université, Pau, France.

2 : TotalEnergies SA, CSTJF, Avenue Larribau, 64000 Pau, France

3 : Géosciences Rennes, Université de Rennes, CNRS, UMR 6118, 35000 Rennes, France

4 : Institut de Recerca Geomodels, Departament de Dinàmica de la Terra i de L'Oceà, Universitat de Barcelona (UB), C/Martí i Franquès s/n 08028 Barcelona, Spain.

** Corresponding author. E-mail address: kalifi.amir@gmail.com (A. Kalifi).*

Abstract

To assess the influence of growing salt structures on facies distribution, stratal pattern, and thickness trends, this paper provides the tectonostratigraphic framework of the outstandingly exposed Cotiella minibasins (South-Central Pyrenees, Spain). Based on detailed analysis of field cross-sections, our results showcase the syn-halokinetic upper Coniacian-lower Santonian Cotiella minibasins infill (1.5-3 km thick) records four shallow-marine depositional sequences, made of mixed siliciclastic-carbonate stratigraphic sequences. This infill is subdivided in three tectonostratigraphic units, identified by using large and small-scale halokinetic structures (i.e. wedges, megaflaps) and variations in facies associations, thicknesses, stratal patterns from the salt wall flanks to the central part of the minibasins. The first unit records the onset of salt movement with overlying laterally continuous sheet-like sedimentary layers and progressive facies transitions over distances of kms. The influence of halokinesis on sedimentation patterns was minor, and only impacted thickness trends and depocenters localization. The second unit records salt evacuation at the surface with the presence of salt-wall derived detritus, the rapid downbuilding and a increase of sand-rich facies proportions. The stratal pattern is characterized by sheet like layers, laterally discontinuous over distances of 300 to 600 meters downdip to the salt wall. Topographically elevated salt walls likely amplified tidal currents, implying sand-rich facies accumulation along the salt wall margin. The halokinesis influence on sedimentation, thickness trends and depocenter localization was significant. The third unit records the end of the salt evacuation stage, marking a brutal decrease of sand-rich facies , likely controlled by regional controls such as eustacy and tectonics. The influence of halokinesis on sedimentation patterns, thickness trends, large-scale geometries and depocenter localization was significant. Our work indicates that distinguishing these large-scale tectonostratigraphic units and their characteristics is of prime importance to understand the archetypal facies distribution, thickness and stratal patterns along salt structures margins.

Keywords

Facies distribution, salt-wall flanking strata, halokinesis, minibasin, stratal pattern, Cotiella Basin.

1. Introduction

Salt tectonics (halokinesis) refers to deformation involving evaporitic rocks: how and when salt structures evolve, the three-dimensional architecture that result from the deformation,their interactions with regional tectonics and contemporaneous sedimentation (e.g. Jackson and Hudec, 2017). In salt minibasins (MBs), defined as 'small intrasalt basin largely surrounded by and subsiding into relatively thick allochthonous or autochthonous salt' (Hudec et al., 2011), salt-sediment interaction control the stratal geometries of sediment layers, related to salt movement (i.e. halokinetic structures). These salt-sediment interaction are primarily controlled by the interplay between volumetric diapiric rise rate and sediment accumulation rate (e.g., Banham and Mountney, 2013; Giles and Rowan, 2012; Pichel and Jackson, 2020), the type of sedimentary environment (i.e. continental or marine depositional environments/siliciclastic or carbonate sedimentation), the structural setting (i.e. compression or extension) and sea-level fluctuations. Throughout the evolution of salt basins, salt-induced depocenters and growing salt structures generates salt-related topographic highs and lows that controls the thickness, location, facies partitioning and internal architecture of stratal packages, (e.g., Barde et al., 2002; Giles & Lawton, 2002; Rowan et al., 2003; Smith et al., 1993; Vendeville & Jackson, 1991). In order to characterize stratal pattern and related facies distribution associated to halokinetic structures, and therefore, increase our predictability of traps and seals (for hydrocarbon production, CO_2 storage, …), outcrop analog studies of halokinetic strata are essential (e.g. Sivas Basin, Turkey: Ribes et al., 2015, 2017, 2018; Kergaravat et al., 2016, 2017; La Popa Basin, Mexico; Andrie et al., 2012; Aschoff and Giles, 2005; Giles and Lawton, 2002; Shelley and Lawton, 2005; Paradox Basin, USA; Hartley and Evenstar, 2018; Jobe et al., 2020; Lawton et al., 2015; Lawton and Buck, 2006; Matthews et al., 2004, 2007; Trudgill, 2011; Flinders ranges, Australia; Collie and Giles, 2011; Gannaway et al., 2014; Kernen et al., 2012; Pyrenees Gannaway et al., 2022; Poprawski et al., 2016, 2014; Roca et al., 2021; Alps ; Célini et al., 2022, 2021, 2020; Csicsek et al., 2022; among others). Outcrop analog, as they provide high-resolution sub-seismic scale information, permit to unravel the interplay between salt rise rate and sedimentation rate, thereby offering keys to better predict spatial and temporal evolution of reservoir properties. This paper addresses the following key questions:

- How does regional tectonics and eustacy control accommodation and sediment input to create MBs?
- How do the relative rates of sedimentation and salt rise rates influence/control the stratigraphic geometry and consequently, the facies distribution?
- How does the interplay between the type of MB, the type of salt structure and the region structural setting impact shallow-marine sedimentation?

The Cotiella Basin, in the South-Central Pyrenees (Spain) allows to address these questions with outcrop exposures of seismic scale MBs that developed on the Triassic salt during the post-rift evolution of the Pyrenees (e.g. Lopez-Mir et al., 2016a, 2016b, 2015). Cotiella MBs are outstandingly exposed to study salt-sediment interaction from extensive three-dimensional exposures of shallow marine mixed siliciclastic-carbonate syn-halokinetic strata (up to 1500 m thick). The main steps of this paper are to: (1) reconstruct sedimentation patterns recorded by the syn-halokinetic strata of the Cotiella MBs; (2) propose a revised sequence stratigraphic framework to better understand the timing of salt-induced geometries and depocenters migrations, thereby leading to a proposition of a detailed tectono-sedimentary evolution of the Cotiella MBs; (3) determine the controlling factors of the spatial and temporal sediment distribution in salt MBs (i.e. halokinesis vs external factors).

2. Geological setting

The tectonostratigraphic sequences exposed in the Pyrenees witness the evolution of a complete orogenic cycle, starting from the opening of the central Atlantic and Bay of Biscay oceanic realm during Late Jurassic-Early Cretaceous and ending with the collision between the Iberian and European plates during Late Cretaceous to Miocene (e.g., Macchiavelli et al., 2017; Muñoz, 1992; Rosenbaum et al., 2002). This study focuses on the post-rift Late Cretaceous Cotiella Basin which were transported by the Cotiella-Bóixols thrust sheet during late Santonian to late Maastrichtian times (McClay et al., 2004; Fig. 1A, B, C).

The stratigraphic succession of the Cotiella Basin starts with Keuper evaporites characterized by red, green and grey gypsiferous clays and gypsum, locally intruded by dolerites sills (Souquet, 1967; Fig. 1D). These sediments are uncomformably overlain by the Upper Cretaceous post-rift succession (Fig. 1D). This succession correspond to the upper Albian to lower Coniacian mainly constituted by carbonate sediments (Turbón, Santa Fe, Pardina and Congost Fms). The post-rift succession continues with the middle Coniacian to lower Santonian sandy calcarenites (Angon-Maciños Fms) and carbonates (Aguasalenz Fm) (Lopez-Mir et al., 2015).

In the Cotiella Basin, the upper Albian to lower Coniacian succession supposedly predate the halokinesis, as they are relatively homogeneous in thickness and facies (García Senz, 2002; Lopez-Mir et al., 2015). The middle Coniacian to lower Santonian sandy calcarenites are interpreted as syn-halokinetic strata (Lopez-Mir et al., 2015). These formations display significant thickness variations, especially at close proximity to the Cotiella thrust (Fig. 1C) interpreted as a partially inverted gravity-driven extensional fault (Lopez-Mir et al., 2016a). There, the thickness of the middle Coniacian to lower Santonian syn-halokinetic succession was estimated at 6 km (Lopez-Mir et al., 2015), while these sediments are only 300 m thick in the footwall of the Cotiella thrust (García Senz, 2002; McClay et al., 2004).

The Cotiella Basin is composed of four MBs, namely Cotiella, Armeña, Mediodía and Seira (Fig. 1C). The Cotiella MB is 15 km long and 4 km large and is located between the San Marcial graben to the WNW, the Esera fault to the ESE, the Armeña/Seira MBs to the North and the Cotiella thrust to the South which correspond to the Cotiella partially inverted gravity-driven extensional fault (Lopez-Mir et al., 2016a) (Fig. 1C). This MB exhibits a thickening wedge towards S-SW interpreted as being mainly controlled by the Cotiella gravity-driven extensional growth faulting (Lopez-Mir et al., 2016b, 2015). Nevertheless, the westward-directed migration of the main depocenter of the Cotiella MB during middle Coniacian–early Santonian was interpreted as the result of an along-strike salt expulsion (Lopez-Mir et al., 2016a). To the north, the smaller Armeña, Mediodía and Seira MBs are ~2-3 km large and ~4-5 km long (Fig. 1C) and are bounded to the SSW, by ~NW-SE striking welds, except the still preserved salt wall separating the Armeña and Mediodia MBs (Figs. 1C, 2). The salt structures were initially corresponding to salt walls genetically linked spatially and temporally with gravity-driven extensional growth faulting (Lopez-Mir et al., 2016b, 2015), and controlling sedimentary thickening wedges.

These MBs were initially interpreted as the stratigraphic response to listric normal faulting detached above the Upper Triassic evaporites during post-rift gravity-driven extension (García Senz, 2002; McClay et al., 2004). However, based on the occurrence of both halokinetic structures and the reworking of Keuper evaporites, Lopez-Mir et al. (2016b, 2016a, 2015) refined this scenario model by the incorporation of passive diapirism along salt ridges isolating the MBs and controlling the sediment accumulation and the facies distribution. At the bottom of MBs, formation of salt welds (i.e. surface or thin zone marking a vanished salt body, resulting from complete or nearly complete loss of salt by creep or dissolution; Jackson and Hudec, 2017) occurred after passive halokinesis (Lopez-Mir et al., 2015). Finally, the salt walls separating the MBs were squeezed and the MBs were partially or totally welded in response to the Pyrenean compression (Lopez-Mir et al., 2016a).

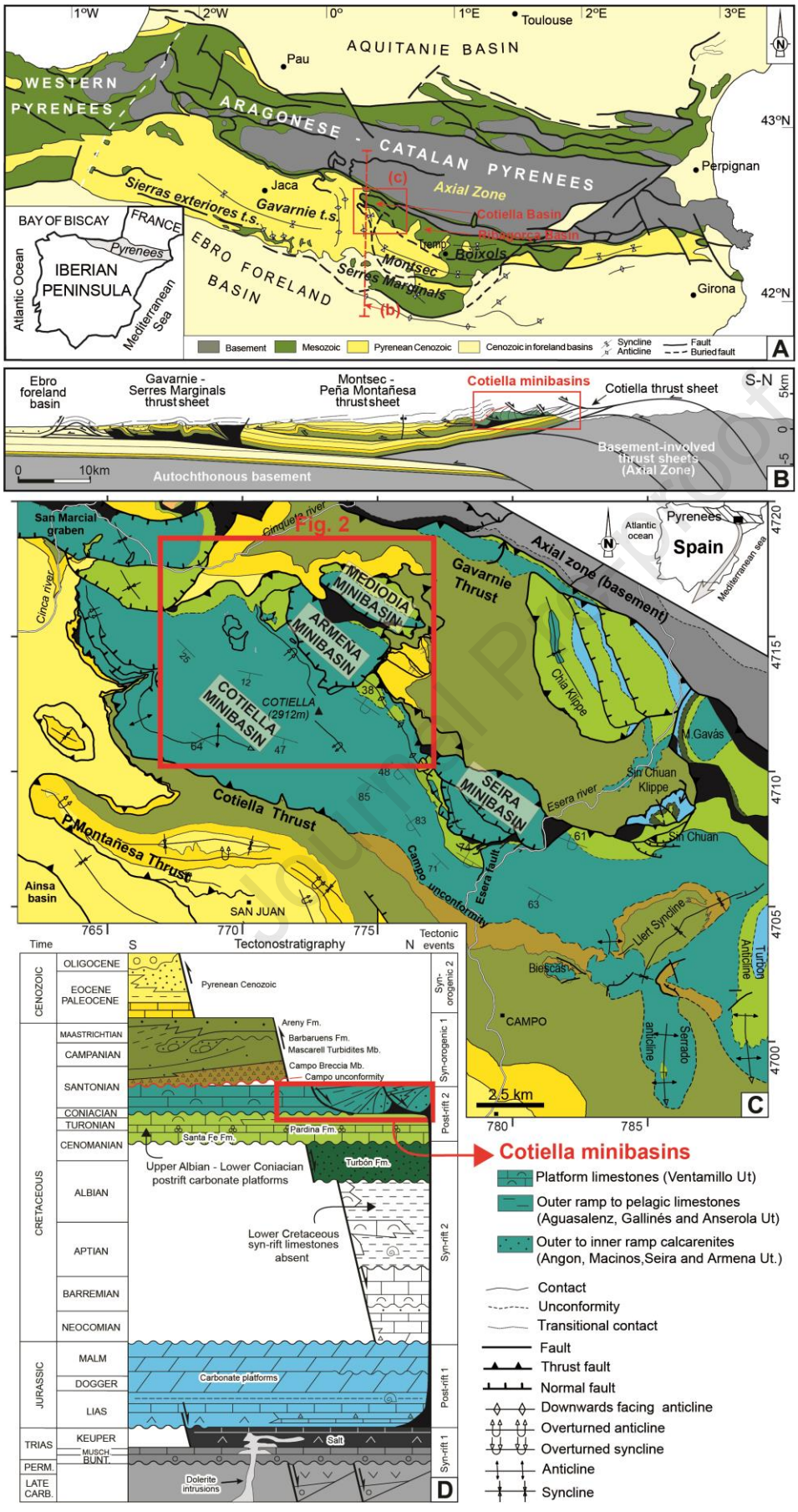

***Figure 1**: (A) Structural sketch showing the location of the Cotiella Basin in the south–central Pyrenees (redrawn from Muñoz, 2002). (B) Regional cross-section showing the main structural elements as well as the Cotiella MBs of the Cotiella Basin along the western portion of the South-central Pyrenean thrust system (redrawn from Lopez-Mir et al., 2016a). (C) Geological map of the Cotiella thrust sheet, indicating the main structural features. (modified from Lopez-Mir et al., 2015). (D) Chronostratigraphy of the of the South-central Spanish Pyrenees and the main tectonic events (redrawn from García Senz, 2002; Lopez-Mir et al., 2015). Detailed stratigraphy of the Cotiella MBs is presented in Fig. 2.*

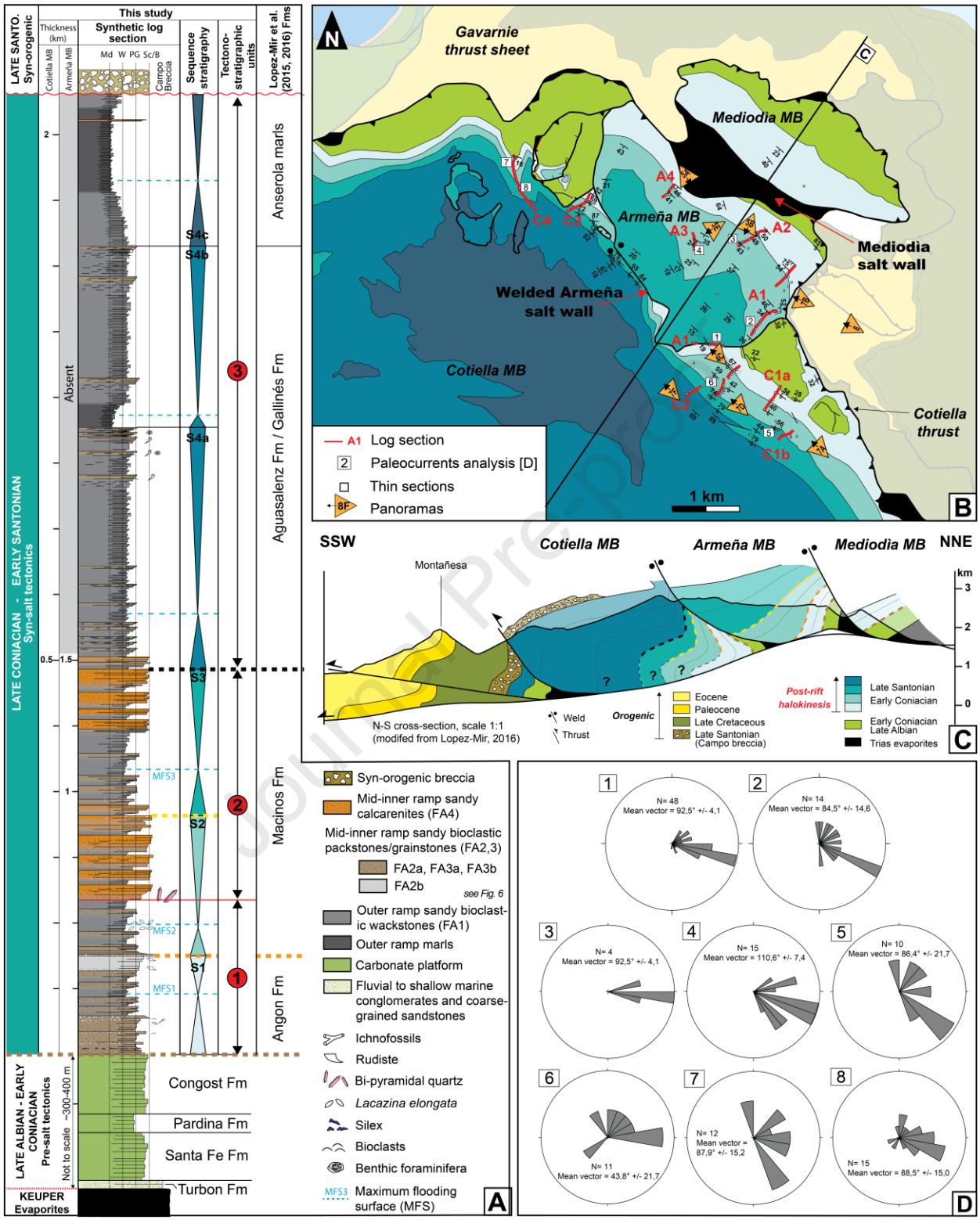

***Figure 2**: (A) Stratigraphy of the Cotiella MBs and comparison with Lopez-Mir et al. (2016b, 2016a, 2015) stratigraphy. Triangle pointing upward (i.e. transgressive system tract) overlain by a triangle pointing downward (i.e. regressive system tract) correspond to one depositional sequence. The red line within the S2 HST strata of the stratigraphic section correspond to the bi-pyramidal quartz rich marker level. Md=*

Mudstone, W= Wackestone, PG= Packstone-Grainstone, Sc= Sandy calcarenite, B=Breccia. (B) Geological map of the study area including the Mediodía, Armeña and Cotiella MBs. The studied log sections and the presented panoramas are localized. See Fig. 2A for the legend of the stratigraphy. (C) NNE-SSW cross-sections throughout the Mediodía, Armeña and Cotiella MBs modified from Lopez-Mir et al. (2016b). (D) Paleocurrent analyses from the S2 and S3 depositional sequences of the Armeña and Cotiella MBs plotted as rose diagrams. Localization of each spot by white square in Fig. 2B. N=number of measurements.

3. Data & Methods

This study is based on detailed analysis of field cross-sections of the upper Coniacian-lower Santonian syn-halokinetic sedimentary successions of the Cotiella and Armeña MBs.

Eight stratigraphical sections containing detailed sedimentological datas across the MBs were logged at a decimeter to meter scale, corresponding to a cumulative thickness of more than 4 km (Fig. 2B). In order to perform the macrofacies and microfacies analysis, 393 samples were acquired along the logged sections and in between, and 96 thin sections were studied. Detailed macroscopic and microscopic sedimentological descriptions were based on stratigraphic surfaces, sedimentary structures and paleocurrents measurements, textural characteristics, clastic and biogenic components. These analyses were integrated to define the lithofacies and their corresponding facies associations, as well as extracting the stratigraphic architecture within and between the mini basins. Petrographic description of the limestones follows the Dunham (1962) classification, except for the sandy calcarenites. The described lithofacies types are grouped into facies associations (FA) according to their interpreted depositional environments. Paleocurrents expressed by cross-bedding forsets have been measured, with the mean vectors of each sites calculated using Lindholm (2012) methodology.

Based on the vertical evolution of FA and stratigraphic surfaces, high-resolution sequence stratigraphy was then applied based on the Embry and Johannesen (1992) methodology. This allows us to (i) describe the stratigraphic architecture of sedimentary systems and define a facies model, and to (ii) identify correlative surfaces (i.e. isochronous Cotiella basin-wide time-lines delimiting genetically related stratal packages) link to autogenic (halokinesis) or allogenic controls (basin-scale tectonic event or eustatic variations). Large-scale genetically related Transgressive-Regressive stratal packages are referred here as depositional sequences including times lines as maximum flooding surfaces (MFS) and sequences boundaries (SB).

Finally, the sedimentological and stratigraphical observations were incorporated to subregional-scale DJI Mavic Pro 2 drone imagery and satellite images in order to better characterize the genetic link between halokinetic geometries and stratal patterns, facies and thickness variations within and between the MBs. The geological map proposed in this paper (Fig. 2B) was built with the support of satellite views and drone imagery as well as by integrating our sequence stratigraphical interpretations regarding the Angon, Maciños and Aguasalenz formations with the Lopez-Mir et al. (2016b) geological map of the Cotiella basin.

4. Facies analysis

Spatial distribution, outcrop-scale lateral correlation of the beds, detailed facies analysis based on texture, sedimentary structures and lithology led to the recognition of eight lithofacies grouped into four facies associations (FA1 to FA4) showing evidence of a mixed siliciclastic and carbonate depositional system: i) sandy bioclastic wackestones (FA1); ii) sandy bioclastic packstones-grainstones (FA2); iii) sandy bioclastic packstones/grainstones to floatstones/rudstones (FA3), and iv) sandy calcarenites (FA4). The facies association and subordinate facies are summarized in Table 1, whereas the general descriptions and interpretations are presented below.

Subfacies	*Description of the facies association (FA)*	*Diagnostic elements*	*Quartz type*		
FA1 Outer ramp environment			**1**	**2**	**3**
FA1a	**Fine-grained well-sorted sandy bioclastic wackestone** Micritized grains and very fine-grained well-sorted detrital quartz grains (0-10%). Occurrence of sponge spicules, benthic foraminifera (*Textularia*, miliolids), bryozoan colonies and calcispheres. Rare planktonic foraminifera and fragments of bivalves and bryozoans. Locally rich in preserved large bivalves or very rich in recrystallized and/or silicified large benthic foraminifera (*Lacazina elongata)*,	Rare sponge spicules	x		
FA1b		Frequent occurrence of chert and abundant sponge spicules	x		
FA2 Middle ramp environment					
FA2a	**Fine to medium-grained and very-well to moderately sorted sandy bioclastic packstone to grainstone** Abundant rounded to sub-rounded recrystallized and/or rounded micritized grains (undifferentiated bioclasts or pelloids), various proportion of well-sorted sub-angular detrital quartz grains. Locally, bi-pyramidal quartz-grains overgrowths are common. Common well-sorted fragments of bivalves (rudists and others), echinoderm plates, ostracods, red/green algae, brachiopods, gastropods, benthic foraminifera (miliolids, *rotalidae*, *numofolatia*, *textularia*) and bryozoans. The matrix is locally affected by secondary dolomitization.	Well-sorted fine to medium sub-angular detrital quartz grains (10-30%). Abundant micritized benthic foraminifera (> 40%). Brunish colored limestones.	x		x
FA2b		Absence or very rare detrital quartz grains (<10%). Very abundant rudist fragments. Whitish-colored massive limestones. Secondary dolomitization is frequent.	x		x
FA3 Proximal middle ramp to inner ramp environment					
FA3a	**Medium to very coarse-grained and moderately to poorly-sorted packstone/grainstone to floatstone/rudstone** Abundant bioclastic fragments (echinoderm plates, red/green algae, bivalves (rudists, oysters and others), gastropods, brachiopods, bryozoans, corals, stromatoporoids) in various proportion and size (from pluri micro-mm to pluri mm). Preserved or broken large benthic foraminifera (*Praealveolina*, *miliolides*) are common. Locally, bi-pyramidal quartz-grains overgrowths are rare. Very poorly sorted fine to coarse-grained detrital quartz (10-30%) and frequently very-coarse-grained sub-angular « local »	Brunish-colored limestones, occasionally evolve to a floatstone, grains are medium to coarse-grained, and are locally rich in very-coarse to pebbled quartz grain (“local”).	x	x	x
FA3b		Reddish-colored very-coarse to coarse-grained limestone, occasionally evolve to a rudstone breccia. High proportion of mm to pluri-mm bioclastic components, large benthic foraminifera	x	x	x

	quartz. Presence of coarse sub-rounded reworked lithoclasts (Shales, peloidal limestones, dolostones (Keuper/Muschelkalk?). The matrix and/or bioclasts are frequently ferruginitized and/or dolomitized.	(*Praealveolina*), and coarse-grained reworked lithoclasts.			
FA4 Middle ramp to inner ramp environment					
FA4a	**Fine to coarse-grained well-sorted sandy calcarenite.** 40-60% subangular fine to coarse-grained detrital quartz. Common micritized grains (undifferentiated bioclasts or pelloids), echinids (locally abundant) and recrystallized sub-rounded and benthic foraminifera (*Textularia*, *rotalidae*, *miliolids*). In a lower proportion, broken bioclasts (bivalves, rudists and others, ostracods, bryozoans, red algaes). The matrix is frequently ferruginitized and/or dolomitized.	Medium to coarse-grained sandy calcarenite displaying dm to pluri-dm thick highly bioturbated levels (*Palaeophycus*) alternating vertically with pluri-dm thick oblique tangential stratifications. Occurrence of antidunes.	x		x
FA4b		Fine to medium-grained sandy calcarenites displaying pluri-m (2-5m) scale low-angle tangential stratification that orthogonally correspond to pluri-m (2-5m) trough cross-beds. Locally, 2-5m depth channels were observed.	x		x

***Table 1**: Summary of lithofacies descriptions. Header lines introduce the four different facies associations (FA1 to FA4). Quartz grain description is detailed in paragraph 4.2. Quartz type 1 correspond to well to moderately sorted sub-angular quartz, which may constitute 0 to 60% of the sediments originating from terrigenous inputs from the continent; Quartz type 2 are very poorly sorted medium to pebble quartz-grains, intensely altered, suggesting local reworking; Quartz type 3 correspond to poorly sorted fine to coarse-grained bi-pyramidal quartz-grains overgrowths corresponding to authigenic quartz reworked from the Keuper evaporites.*

4.1. Facies associations

FA1: Outer ramp environment

Observation: The FA1 facies association consists of blue-grey well-sorted wackestone (Fig. 3A) containing variable amounts of well-sorted very-fine bioclasts including fragments of bivalves and bryozoans, detrital subangular fine-grained sands (0-10%) and micritized grains (Fig. 3B). Calcispheres, planktonic and small benthic foraminifera (*Textularia, miliolids*), as well as sponge spicules are common (Fig. 3B). Locally, occurrence of bryozoan colonies as well as recrystallized and/or silicified complete specimens of bivalves and/or large benthic foraminifera (*Lacazina elongata*) were observed (Fig. 3A). Two subfacies are recognized in this facies association FA1. Subfacies FA1a is characterized by a low proportion of sponge spicules and higher proportion of fine-grained sands (~2-10%) whereas subfacies FA1b comprises a higher amount of sponge spicules, a lower proportion of fine-grained sands (<3%) and frequent occurrence of chert.

Interpretation: The structureless fine-grained texture and the biota assemblage (i.e. sponges spicules, bivalves, bryozoan colonies, planktonic foraminifera) suggest marine distal low-energy depositional environments marking the transition from euphotic to oligophotic zones (Pomar et al., 2012). The micritic fraction and the occurrence of fine-grained fragments of bioclasts and quartz might have been mainly supplied by suspension clouds derived from storm reworking in shallower waters, indicating depositional environments close to the storm wave-base which is compatible with an outer ramp mixed siliciclastic carbonate system (Pomar, 2001). This agrees with the occurrence of *Lacazina elongata* which are adapted to clear or agitated water, require normal oceanic salinities and live on carbonate substrate in a waterdepth of 20 to 80 m (Gräfe, 2005).

FA2: Middle ramp environment

Observation: The FA2 facies association consists of a very-well to moderately sorted fine- to medium-grained packstone to grainstone mainly constituted by rounded micritized grains (unidentifiable origin or peloids), and various proportion of well-sorted fine to medium sub-angular detrital quartz grains (0-30%) (Fig. 3C). Subordinately, various proportion of echinoderm plates, micrite-rimmed small benthic foraminifera (*miliolids, rotalidae, Nummofallotia, textularia*), well-sorted and well-rounded fragments of bivalves (rudists and others), gastropods, brachiopods, red/green algae and bryozoans are present. Locally, fine to medium-grained bi-pyramidal quartz-grains are common (Fig. 3E, F). Locally, the micritic matrix is totally or partially recrystallized and/or dolomitized. Two subfacies are differentiated (FA2a and FA2b, Table 1). Subfacies FA2a is characterized by a very high proportion of well-sorted micritized small benthic foraminifera and well-sorted detrital quartz (10-30%, Fig. 3C). Subfacies FA2b is characterized by an abundance of angular to rounded rudists fragments and an accessory content of quartz grains and small benthic foraminifera (<10%, Fig. 3D). FA2b frequently show important secondary dolomitization.

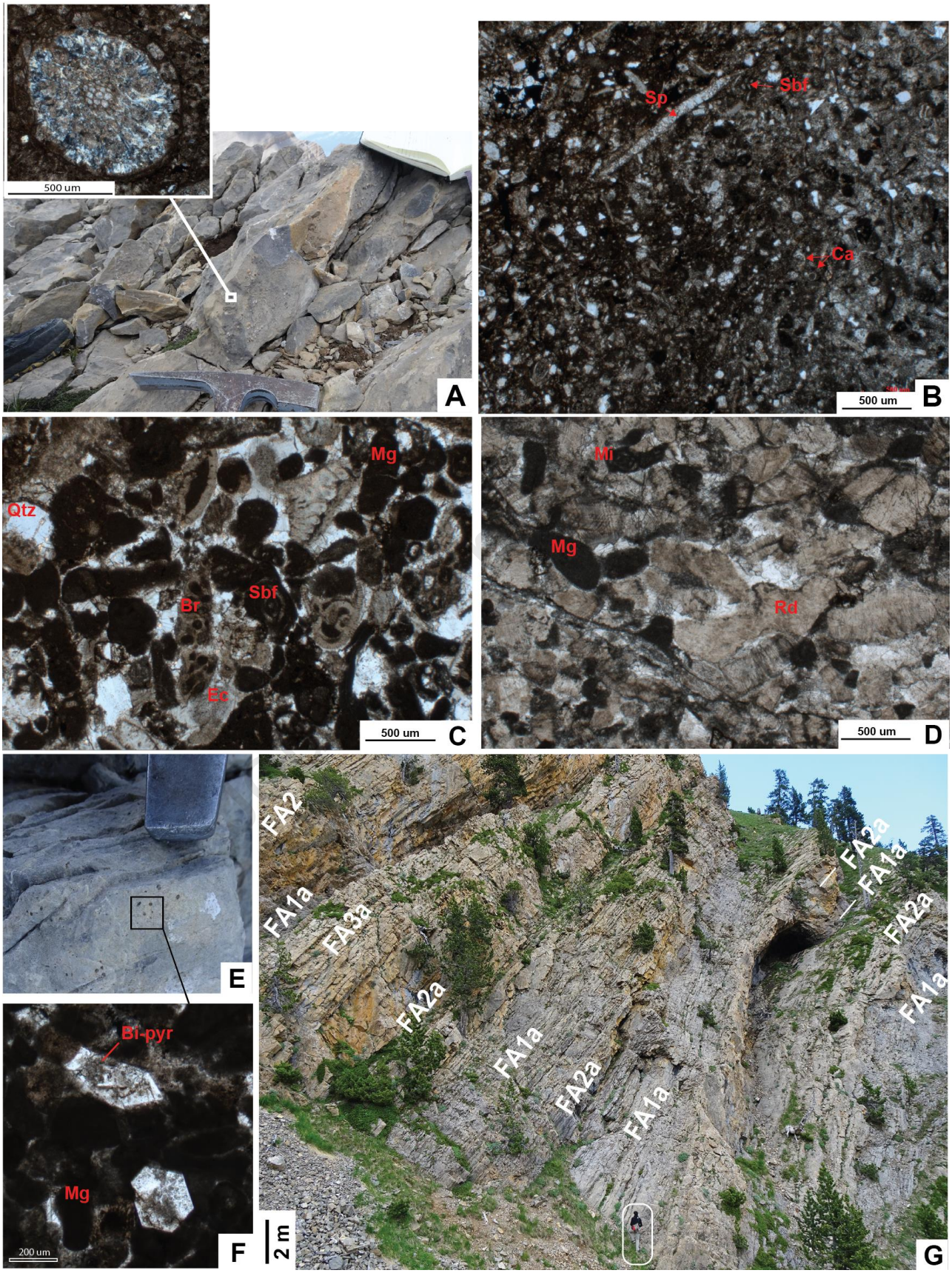
500 um
A
Sp
Sbf
Ca
500 um
B
Mg
Qtz
Br
Sbf
Ec
500 um
C
Mi
Mg
Rd
500 um
D
E
Bi-pyr
Mg
200 um
F
FA2
FA1a
FA3a
FA2a
FA1a
FA2a
FA1a
FA2a
FA1a
FA2a
FA1a
2 m
G

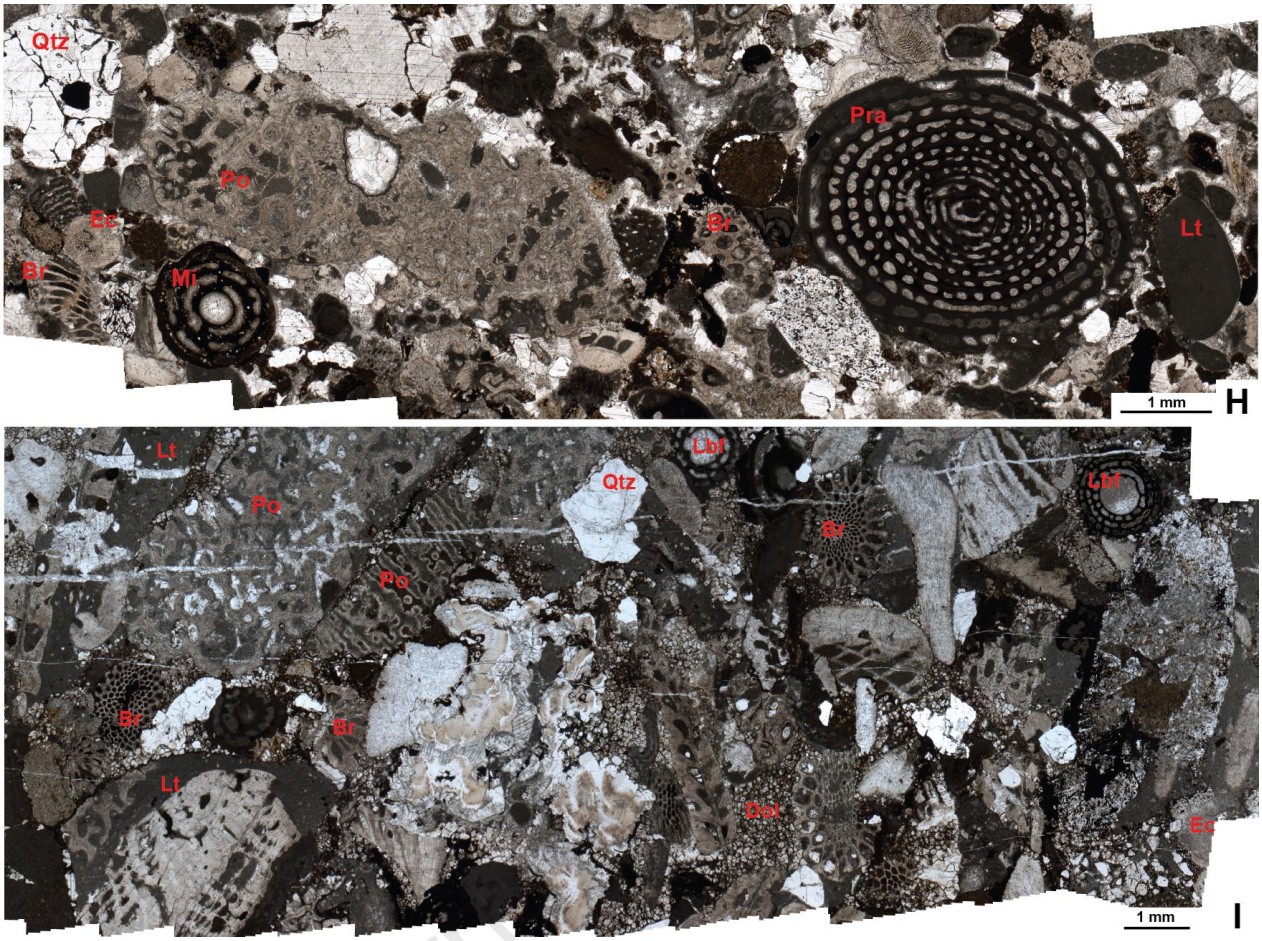

***Figure 3**: Outcrop photographs and thin sections including outer ramp wackestones (subfacies FA1a, FA1b) deposits, middle ramp packstones/grainstones (FA2a-FA2b) to inner ramp floatstone/rudstone (FA3a-FA3b) deposits. Bi-pyr= Bi-pyramidal quartz-grain, Br= Bryozoan fragment, Ca= Calcisphere, Dol= Dolomie, Ec= Echinoderm plate, Lbf= Large benthic foraminifera, Lt= Lithoclast, Mg= Micritized grains; Mi= Miliolidae, Pra= Praealveolina, Po= Porites, Qtz= Quartz, Rd= Rudist fragments, Sbf= Small benthic foraminifera, Sp= Sponge spicule. (A) FA1a macrofacies characterized by abundant Lacazina (close-up view). (B) FA1a microfacies showing occurrence of Ca, Sbf, Sp and very fine-grained quartz within micritic matrix. (C) FA2a microfacies rich in Mg and Sbf. Note the low proportion of quartz. (D) FA2b microfacies exhibiting a richness in Rd. (E) Close-up view on the FA2a bi-pyramidal quartz rich level. Microscopic view in (F), (G) FA1a, FA2a and FA3a macrofacies and vertical evolution along the Armeña Ibon de Plan section (A4). Location in Fig. 2B. (H) FA3a microfacies displaying poorly sorted large bioclastic components as Pra, Br, Mi, Ec. Note the rare proportion of intensely altered quartz-grains. (I) FA3b microfacies displaying very poorly sorted large bioclastic components as Po, Lbf, Br.*

Interpretation: The diversified spectrum of bioclasts made of benthic foraminifera, fragments of bivalves, gastropods, brachiopods, red/green algae and bryozoans, indicates open circulation and a chlorozoan association within the eu-oligophotic zone. The microfacies analysis evidences the coexistence of both preserved (small benthic foraminifera) and abraded components suggesting that biologic components are autochthonous to parautochthonous. The relatively good sorting as well as the sub-rounded fragmented bioclasts suggest high-energy marine depositional environments and intense reworking from shallower

waters which may have been produced by wave/storm or tidal currents (the lack of sedimentary structures observation prevents from a more detailed analysis). This suggests depositional environments between storm and fair weather wave-bases, most probably within a middle ramp hydrodynamic zone (Burchette and Wright, 1992; Civitelli and Brandano, 2005; Pomar, 2001). Subfacies FA2b rich in angular to rounded rudists fragments suggest a proximity to rudist biostromes. The absence of in-situ rudist biostromes nearby the study area might suggest localized biostromes intensely reworked by waves.

FA3: Proximal middle ramp to inner ramp environment

Observation: The FA3 facies association corresponds to a moderately to very poorly-sorted medium to very coarse-grained packstone-grainstone to floatstone-rudstone mainly constituted of variable amounts of various-sized large benthic foraminifera (*Praealveolina*), subangular fragments of brachiopods, crinoids, bryozoans, bivalves (rudists, oysters and others), red and green algae, corals (*Porites*) and stromatoporoids (Fig. 3H, I). The angular to subrounded larger bioclasts may be encrusted by red algae, and/or may be bored by lithophagous bivalves. The facies are also characterized by well-rounded reworked lithoclasts (Fig. 3H, I), which may also be riddled with borings from lithophagous bivalves. Subordinately, the matrix is a poorly sorted packstone to grainstone containing variable amounts of poorly sorted sub-angular quartz ((i) detrital quartz, (ii) medium to granule intensely altered quartz-grains, (iii) fine to coarse-grained bi-pyramidal quartz-grains) micritized grains, small benthic foraminifera (*miliolids, textularia*) and rudists fragments. Two subfacies are differentiated (FA3a and FA3b, Table 1). Subfacies FA3a is medium-coarse grained packstone/grainstone to floatstone and is rich in moderately to poorly sorted, sub-angular, intensely altered quartz pebbles (Fig. 3H). FA3a is characterized by a brunish color while FA3b is reddish (induced by secondary ferruginitization and dolomitization). Subfacies FA3b is a very-coarse grained packstone-grainstone and constitute locally a breccia rudstone facies (Fig. 3I). FA3b is characterized by a high proportion of mm to pluri-mm bioclastic components, large benthic foraminifera (*Praealveolina*), and rounded coarse-grained reworked lithoclasts.

Interpretation: As for FA2, the FA3 facies association presents a diversified spectrum of bioclasts indicating open circulation and a chlorozoan association within the eu-oligophotic zone. The very poorly-sorting facies composed by large, fragmented skeletons and shells suggest high-energy marine depositional environment or high energy events. The subangular shape of the larger bioclasts, the local red algal encrustation and penetration by borings suggest immature reworking (or par-autochthonous origin) from the exposure area of these biologic components. This also indicate continuous or frequent high-energy conditions, suggesting that FA3 were deposited in shallower depositional environments compared to the FA2 middle ramp deposits, most probably close or within the fair weather wave-base and thus, proximal middle ramp or inner ramp depositional environment (Brandano and Civitelli, 2008). This is in accordance with the occurrence of parautochtonous shallow water fauna as large fragments of corals, stromatoporoids and large benthic foraminifera (*Praealveolina*) which are absent in FA2 facies.

FA4: Middle ramp to inner ramp environment

Observation: The FA4 facies association consists of well-sorted fine to coarse arenites composed of both bioclasts and siliciclastic sand. The siliciclastic sand fraction constituted of well-sorted sub-angular monocrystalline detrital quartz grains generally represent more than 40% of the clast fraction (Fig. 4A, B). The bioclastic sand fraction constitutes less than 30% of the sediment and mainly include micritized grains (unidentifiable origin or peloids), echinoids (locally abundant) and small benthic foraminifera (*miliolids, textularia*, *rotalidae* and *Nummafolatia*) (Fig. 4A, B). Subsequently, well-sorted and sub-rounded fragments of bivalves (rudists and others), bryozoans and red algae are present. The matrix is rare but frequently dolomitized and ferruginitized, especially when quartz proportion is high. Two subfacies are

defined (FA4a and FA4b, Table 1). Subfacies FA4a (Fig. 4A) is mainly constituted by medium to coarse-grained sandy calcarenites and display dm to pluri-dm thick highly bioturbated layers (*Palaeophycus*) alternating vertically with pluri-dm thick levels displaying oblique tangential stratifications (Fig. 4C, E, F). These oblique strata exhibit well-preserved foresets and bottomsets of prograding sedimentary structures. Each foreset bed package are pluri-cm to dm-thick and are characterized by an upward fining-up trend, evolving from reddish, coarse-grained, sandy calcarenites to burnish bioturbated, medium-grained, sandy calcarenites (Fig. 4F). A rhythmic pattern in the thickness of foreset bed packages is also observed (Fig. 4F). Opposite-directed cm-scale ripples are locally observed along the foreset laminae (Fig. 4F). Laterally, bottomsets are evolving towards pluri-dm thick undulated laminae characterized by migration of the crests in the opposite direction compared to the foresets. The undulated laminae are also displaying a general decrease in dip on the forward slope, passing to (sub-) planar lamination (Fig. 4G). Subfacies FA4b is characterized by fine to medium-grained sandy calcarenites (Fig. 4B) and may display pluri-m (2-5m) scale trough cross-bedding (Fig. 5A, B, C, E). These structures correspond in the orthogonal section to pluri-m (2-5m) scale low-angle tangential stratification (Fig. 5D). Locally, FA4b is filling a ~5m depth low-angle incision and is laterally discontinuous at tens to hundreds of meters passing distally to fine grained deposits (FA2a or FA1b) and/or proximally to coarser deposits (FA4a) (Fig. 4C, D, E). Most of the cross strata at any location and level show a dominant orientation toward the E-ESE (Figs. 2D, 5B, C, D).

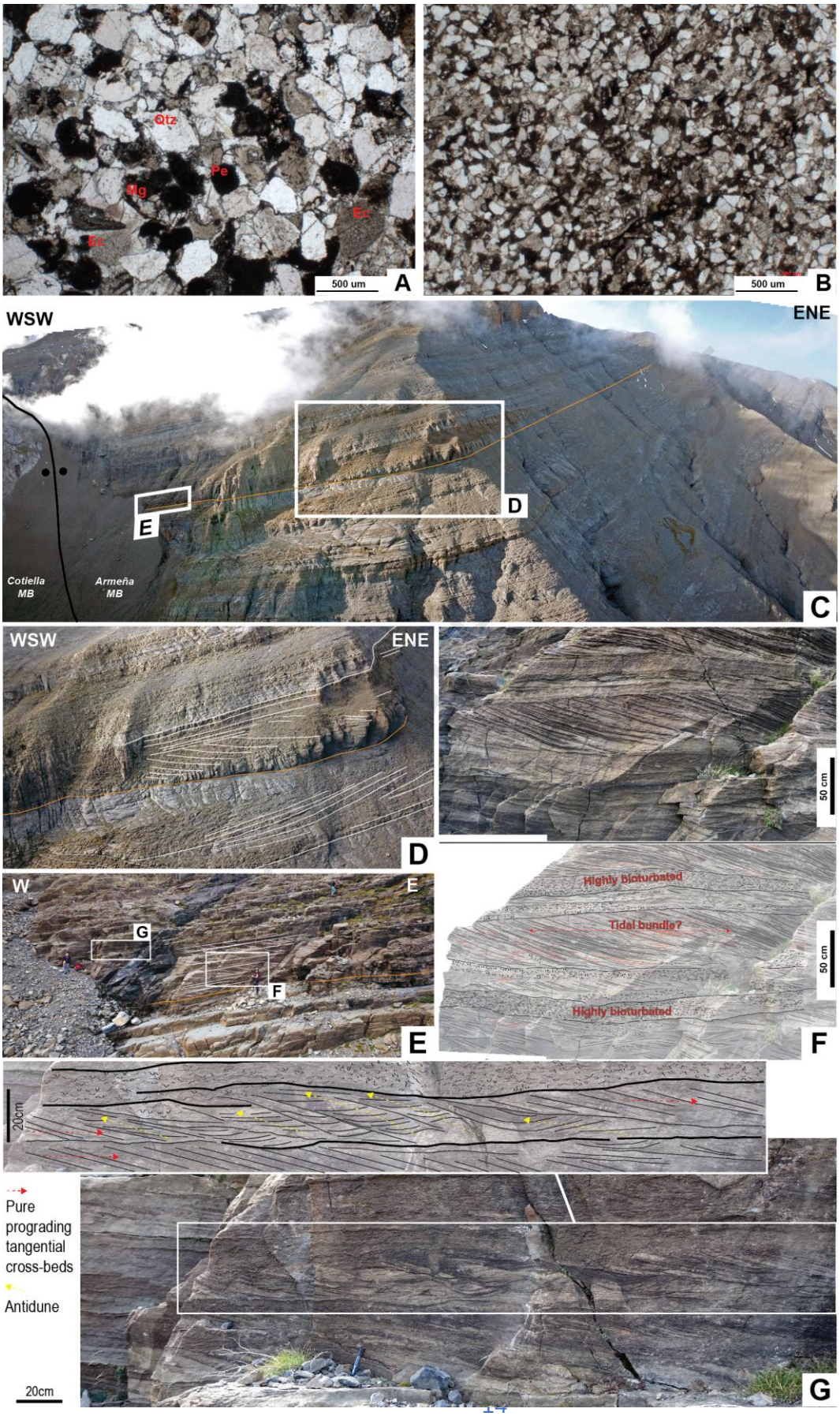
Qtz
Pe
Mg
Ec
Ec
500 um
A
500 um
B
WSW
ENE
E
D
Cotiella MB
Armeña MB
C
WSW
ENE
D
50 cm
W
E
G
F
E
Highly bioturbated
Tidal bundle?
Highly bioturbated
50 cm
F
20cm
Pure prograding tangential cross-beds
Antidune
20cm
G

***Figure 4**: Illustrations of the middle ramp to inner ramp environment FA4a and FA4b subfacies. Qtz= Quartz. Mg= Micritized grain. Ec= Echinoderm plate. Pe= Pellet. (A) Microfacies of the medium to coarse-grained FA4a subfacies and the fine to medium-grained sandy calcarenites FA4b subfacies (B). Note the well-sorting and moderately rounded quartz grains and the low proportion of bioclastic components. (C) Rapid transition between FA4a (E) and FA4b (D) lithofacies along the Armeña weld. (D) FA4b pluri-m scale trough crossbedding is interpreted as tidal channel. (E, F) FA4a dm to pluri-dm thick highly bioturbated levels (Palaeophycus) alternating vertically with pluri-dm thick oblique tangential stratifications characterized by tidal bundles and opposite-directed oblique tangential cm-scale ripples (red lines). (G) Antidunes of the FA4a subfacies. Pen is 12.5 cm long.*

Interpretation: The well-sorting of the sandy calcarenites, the diversified spectrum of marine bioclasts as well as the occurrence of cross-stratified sedimentary structures suggest high-energetic marine depositional environment. Such an interpretation agrees with the dominance of bioclasts fragmentation, the relative enrichment of echinoids resulting from their resistance to mechanical abrasion. The uni- or bi-directionally stacked pluri-dm to pluri-m tangential and/or trough cross strata, suggest 2-D and/or 3-D prograding dunes with a composite lateral accretion (especially for FA4b trough cross-beds). In subfacies FA4a, the occurrence of the rythmic variability in the coarseness and thickness of the tangential foreset bed packages, may correspond to tidal bundles reflecting neap-spring tidal cycles (Ashley, 1990; Boersma, 1969; Kreisa and Moila, 1986; Visser, 1980; Yang and Nio, 1985). This is consistent with the occurrence of opposite-directed tangential ripples preserved along foresets that testify bi-directional currents in response to tidal influence. The prevalently SE/ESE direction of the foresets and the secondary NW/WNW component of the opposite-directed ripples suggest a local asymmetry of the tidal currents. Undulated laminae of FA4a subfacies are attributed to antidunes, formed by supercritical currents (Cartigny et al., 2014) induced possibly during rising or falling spring tides (Dietrich et al., 2016). The pluri-dm height of tidal dunes of FA4a suggest that they were deposited in shallow marine waters (Dalrymple and Rhodes, 1995) that would be equivalent to proximal middle ramp to inner ramp sedimentary environments. This is in accordance with the occurrence of *Paleophycus* ichnofossiles formed mainly in middle shoreface depositional environments (Gérard and Bromley, 2008; Sharafi et al., 2014). The monospecificity of the ichnofaunal assemblage indicates a stressed environment (e.g. de Gibert and Goldring, 2007; Malpas et al., 2005) that agrees with tidal dominated environments. The 2-5m height of tidal dunes and low-angle channel depth (~5m) of subfacies FA4b, suggest that they were deposited in more distal sedimentary environments (water depth <25 m; Dalrymple and Rhodes, 1995) that would be equivalent of a proximal to distal middle ramp hydrodynamic zone. Modern analogs are consistent with this interpretation as cross-bedded deposits described along middle ramp occur at ~40-60m of water depths (e.g. Fornos and Ahr, 1997; Hallock et al., 1988; Pomar, 2001).

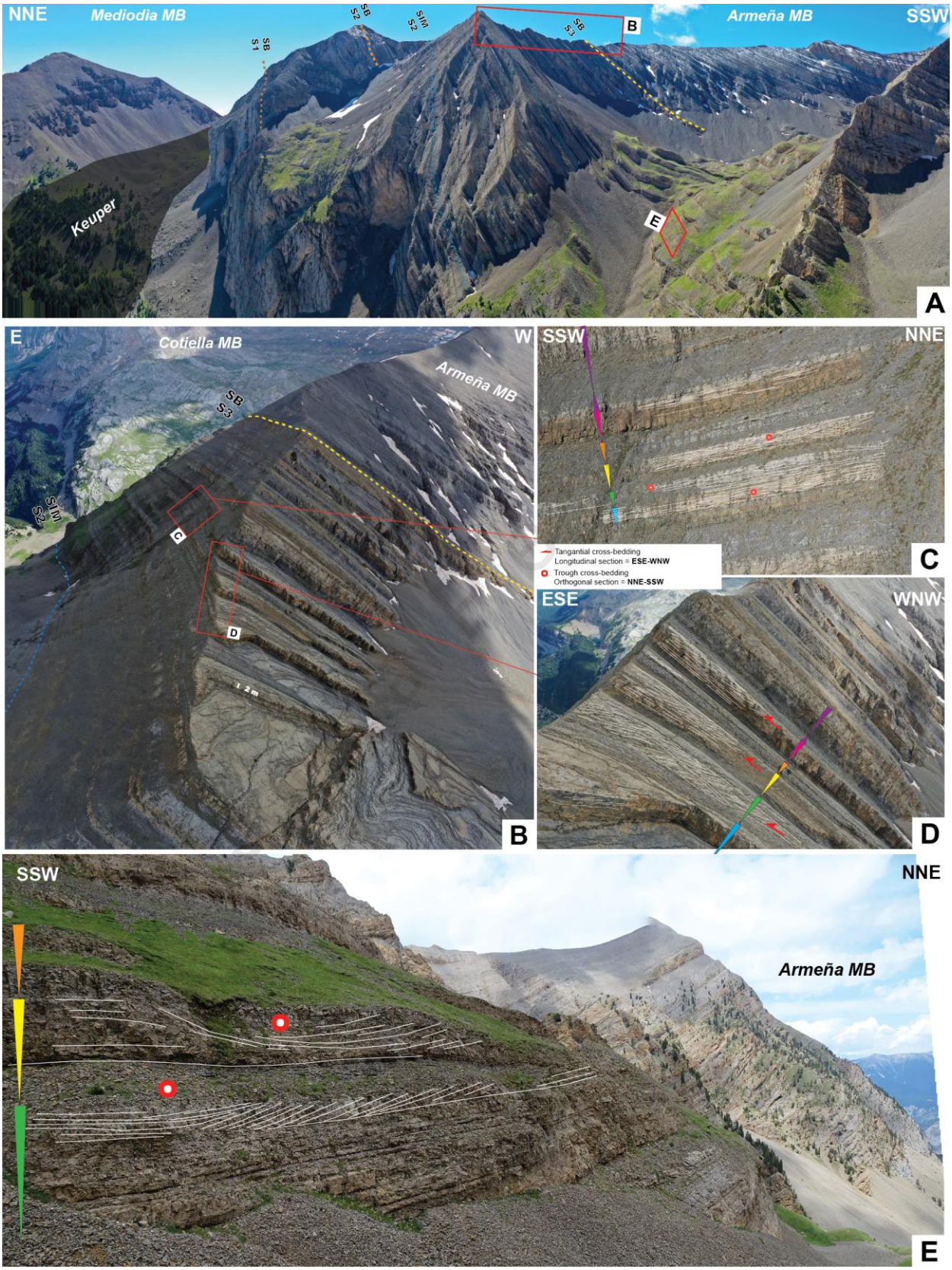

Figure 5: *Panoramas illustrating the spatial distribution of FA4b subfacies in the distalmost exposed area*

of the Armeña MB. See Fig. 2B for viewpoints localisations. (A, B) Stratigraphical context of the illustrated parasequences. Pluri-m scale low angle trough crossbedding (C, E) that orthogonally correspond to pluri-metric low angle tangential crossbedding prograding towards ESE (D).

4.2. Detrital grains description

Based on petrographical microtextures analyses of the 4 facies associations, three different types of quartz grains were identified through the MBs infill (Table 1). Their interpretations indicate different provenance source.

(i) type 1 corresponds to well to moderately sorted sub-angular detrital quartz and were observed in the 4 FAs. Type 1 quartz grains may constitute 0 to 60% of the sediments (Figs. 3B, C; 4A, B). The well sorting results either from wave, tidal and/or fluvial action prior to deposit. The subangular shape, as well as large volume of sand sedimented within the studied sedimentary succession indicates that type 1 siliciclastic grain is most probably originates from terrigenous inputs from the continent (i.e. Ebro massif). Another possibility could be the reworking of the Triassic sandstones (i.e. Buntsandstein). These latest were probably exposed to the south, where they are outcropping on top of the footwall of the inverted Cotiella extensional fault, which corresponded initially to the southern boundary of the Cotiella Basin (Lopez-Mir et al., 2015).

(ii) type 2 consists of very poorly sorted medium to granule-size quartz grains, and were observed only in the FA3 facies association. The poor sorting, the internal fractures (Fig. 3E), the rare association with recrystallized feldspars and the abraded borders points out to a source area with reworking of Hercynian basement and/or Turbon Fm conglomerates and sandstones (Fig. 1D). During Upper Coniacian-Lower Santonian, the Hercynian basement were probably outcropping to the south, again, on top of the footwall of the inverted Cotiella extensional fault (Lopez-Mir et al., 2015).

(iii) type 3 corresponds to poorly sorted fine to coarse-grained bi-pyramidal quartz crystals (Fig. 3 E, F) resulting from overgrowths induced by diagenetic replacement of anhydrite nodules within the Triassic evaporites. These quartz were observed in the FA2, FA3 and FA4 facies associations. These authigenic quartz are reworked from the Keuper evaporites, and are known in the Pyrenees and the Iberian range as the "*Jacintos de Compostella*" Gómez-Alday et al., 1994a, 1994b; Lopez-Mir, 2013) (Gómez-Alday et al., 1994a, 1994b; Lopez-Mir, 2013; Querol et al., 1992). They are currently interpreted as diapir-derived detritus where the evaporitic constituents are readily dissolved or altered during diapir exposure. The stable quartz crystals are commonly recycled into diapir-flanking strata and have recently been used to document passive diapir growth of Keuper evaporites in the Ribagorçana Basin (Southern Pyrenees, Gannaway et al., 2022; Fig. 1A for location).

5. Depositional systems and stratigraphic evolution of the Cotiella MBs

Conformably above the upper Albian-lower Coniacian pre-halokinetic units, the upper Coniacian to lower Santonian succession of the Cotiella and Armeña MBs is subdivided into four depositional sequences (Fig. 2A). This sequence-stratigraphic framework was achieved using correlation of parasequence stacking pattern and key surfaces. The parasequence stacking pattern allowed the identification of depositional sequences (and system tracts) based on retrogradational, progradational and aggradational parasequence

stacking patterns (Fig. 2A). The key surfaces (detailed in paragraph 5.2) include (1) sequence boundaries (SB), (2) maximum flooding surface (MFS), and (3) a bi-pyramidal quartz rich level, which materializes a recognizable timeline along the Cotiella and Armeña MBs successions.

5.1. Depositional Systems

The facies associations (FAs) evidenced through the Cotiella MBs display successive depositional environments characterizing an overall mixed siliciclastic-carbonate depositional system. The four FAs are internally organized as 5 to 30m-thick parasequences (Fig. 6). Facies evolution in the individual parasequences indicates shallowing-upward trends of depositional conditions, from fine-grained distal low energy outer ramp deposits (FA1) to coarsest, shallowest and highest-energy middle to inner ramp deposits (FA3, FA4), respectively. Evidence of emersion has never been observed and the parasequences boundaries are indicated by significant environmental change, from shallow shoals to relatively deeper outer ramp environments, corresponding to marine flooding surfaces. Based on the vertical facies assemblages and their spatial distribution along proximal to distal transects (applying Walther's law), two types of parasequences were described, materializing two distinct depositional systems alternating through time (Fig. 6): (i) a carbonate-dominated mixed system and a (ii) terrigenous-dominated mixed system. The carbonate-dominated mixed system (FA1, FA2 and FA3) can be replaced along a proximal-distal depositional profile, as described in Burchette and Wright (1992). The terrigenous-dominated mixed system, in view of the classification of terrigenous dominated tidal depositional environments due to Dalrymple and Rhodes (1995), facies associations FA1, FA2 and the terrigenous and tide dominated FA4 facies association can be replaced along a proximal-distal depositional profile.

The main difference between these two systems is the highest proportion of siliciclastic components in the terrigenous dominated mixed system. The stratigraphic organization and evolution between these two systems is detailed below.

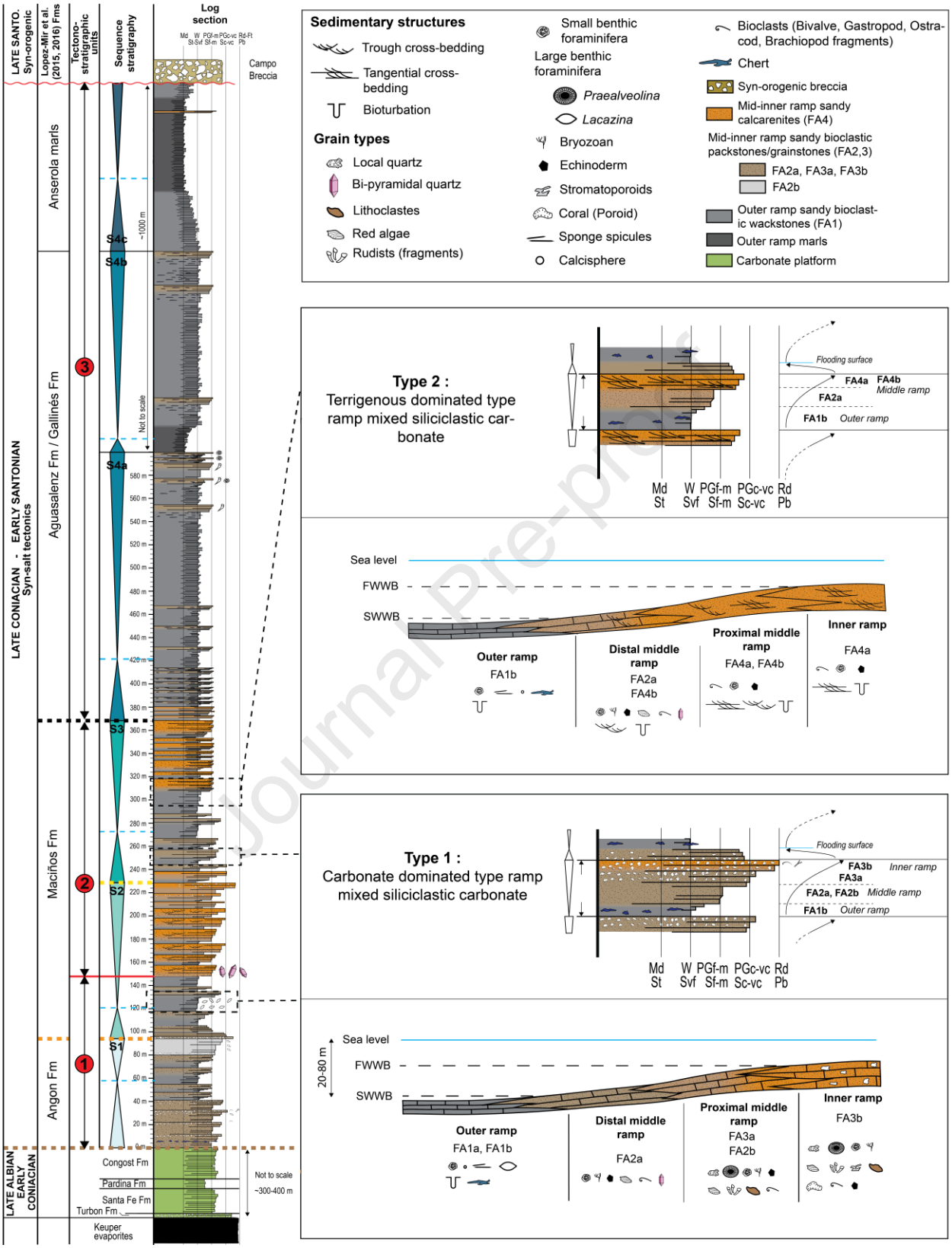

Figure 6: *Depositional models of the terrigenous (type 2) and carbonate-dominated (type 1) type ramp mixed siliciclastic carbonate environments of the Upper Coniacian to Early Santonian succession of the*

Cotiella MBs. The red line within the S2 HST strata of the stratigraphic section correspond to the bi-pyramidal quartz rich marker level.

5.2. Stratigraphic succession and key surfaces

Four depositional sequences (S1, S2, S3 and S4) were described within the Cotiella and Armeña MBs (Figs. 2A, 6).

S1 sequence (~Angon Fm *sensu* Lopez-Mir, 2013): The S1 depositional sequence is characterized by a lowermost aggradational to a retrogradational (TST) and an upper progradational (HST) carbonate dominated parasequence set pattern (Figs. 2A, 6). The lowermost aggradational parasequence set and the overlying retrogradational pattern are capped by the maximum flooding surface (MFS S1). The overlying progradational pattern (HST) is characterized by a richness in rudist fragments (FA2b subfacies representing shallowest term of the parasequences) indicating reworking from local build-ups.

S2 sequence (~Lower Maciños Fm *sensu* Lopez-Mir, 2013): The S2 sequence boundary (SB) is marked by the appearance of a 50 cm to 1 m thick monogenic lag, rich in very poorly sorted medium to pebble type 2 quartz pebbles (Fig. 2A) and suggesting intense reworking during the initial transgression. In the Armeña MB, this marker level was recorded only along the welded Armeña salt wall (A1 log section, Fig. 2B). The S2 depositional sequence is characterized by a lowermost retrogradational pattern (TST) and an uppermost progradational pattern (HST). In both MBs, the TST is characterized by carbonate dominated parasequences. The maximum flooding deposits bounding the TST and the HST of the S2 sequence is a marker level characterized by an abundance in *Lacazina elongate* large benthic foraminifera (Figs. 2A, 3A), which indicate maximum water depth of 80 m (Gräfe, 2005). During the lowermost deposits of the HST, immediately or few meters above the MFS, an easily recognizable marker level characterized by a bi-pyramidal quartz-rich sedimentary layer is observed (Figs. 2A, 3E, F). The latter seems to be synchronous to thickness variation within the hangingwall of normal faults likely compatible with growth strata in response to normal fault activity. These syn-sedimentary extensive faulting were observed for both the Armeña MB (with ~NW-dipping normal faults) and the Cotiella MB (~NNE-dipping normal faults) and suggest a ~N-S directed extension. However, a detailed structural analysis is needed to better characterize this deformed interval and its impact on the stratal pattern and the reservoir facies distribution along salt structures. The bi-pyramidal quartz indicates most probably that these extensive structures are coeval with reworking of Keuper evaporites and thus, the onset of salt evacuation. Moreover, this marker level highlights the brutal appearance of (i) terrigenous-dominated parasequences (Fig. 6) and (ii) chert-rich fine-grained outer ramp facies (FA1b).

S3 sequence (~Upper Maciños Fm *sensu* Lopez-Mir, 2013): The SB of the overlying S3 sequence is a marker level characterized by a brutal inversion between the underlying progradational parasequence set pattern of the S2 HST, and the overlying S3 retrogradational parasequence set pattern (S3 TST). The S3 is characterized by both, the terrigenous dominated and carbonate dominated parasequences (Fig. 6). During S3 HST depositional sequences, uppermost deposits of each parasequences display important spatial variability and are (i) pebbly to very coarse-grained in the easternmost part of the Cotiella MB, (ii) fine-grained in the westernmost part of the Cotiella MB, and (iii) medium to coarse-grained in the Armeña MB.

S4 sequence (~Aguasalenz, Gallinés and Anserola marls Fms *sensu* Lopez-Mir, 2013): The overlying S4 sequence only exists in the Cotiella MB and consists of a very thick succession (at least 1500m-thick, Fig. 2A) mainly constituted by distal outer-ramp fine-grained blue grey wackestones deposits. Based on the C4

section (Fig. 2B) combined with Pascual-Cebrian (2009) Gallinés section, the S4 sequence is internally subdivided into 3 shallowing upward sequence (S4a, S4b, S4c). Each of them is internally organized as a stack of sandy or carbonate dominated parasequences, characterized by very high proportion of fine-grained, outer ramp facies (Fig. 6). The S4a and S4b sequences corresponds to the Aguasalenz Fm in the eastern part of the Cotiella MB and to the Gallinés Fm in the western part (Lopez-Mir et al., 2016a, 2015). S4c sequence marks the onset of the Anserola marls constituting the uppermost part of the syn-halokinetic strata of the Cotiella Basin. This last unit was defined by Mey et al. (1968) and is made up of centimetric to decimetric rhythmic grey nodular marls with sporadic flint nodules, with abundant echinoderms (Souquet, 1967) and inoceramids, indicating a depositional environment in the transition of the inner to the outer ramp.

Paleocurrent directions were measured at 8 sites located throughout the tide-dominated sandy-rich facies (FA4, Fig. 6) deposited during S2 and S3 depositional sequences in the two studied MBs. Paleocurrents are largely directed to the ~E-ESE, except for sites n°5 and 7, where paleocurrents are directed to the ~SE-SSE (Fig. 2B, D). No major changes in the paleocurrent directions were observed trough time.

By combining lithofacies assemblage type (i.e. type 1 or type 2 parasequence type, Fig. 6), lithofacies distribution trend type (i.e. rapid changes or lateral continuity) and the stratal pattern type (i.e. asymmetric stratal thickening adjacent to salt diapirs or relatively uniform stratal thickness), we have subdivided the syn-kinematic stratal packages of the Armeña and Cotiella MBs in three tectonostratigraphic units: (i) Unit 1 includes the S1 depositional sequence strata and the S2 strata comprised between S2 sequence boundary and the bi-pyramidal quartz rich marker level, (ii) Unit 2 includes the strata comprised between the bi-pyramidal quartz rich marker level and the S4 sequence boundary. The bi-pyramidal quartz rich marker layer marks an abrupt change in the sequence stratigraphic architecture and facies assemblage of the succession, from underlying wackestones-dominated units to an abrupt increase of the sand-prone facies. This transition results from the appearance of type 2 terrigenous-dominated parasequences (Fig. 6). Finally, (iii) Unit 3 corresponds to the S4 depositional sequence (Figs. 2A, 6).

6. Influence of halokinesis on the Cotiella minibasins

The infill of the Cotiella MBs shows rapid changes in thickness from one MB to another (Mediodía, Cotiella and Armeña), with spectacularly well exposed stratal patterns expressed by wedges, megaflap geometries along salt walls, or welds (Hudec et al., 2011; Hudec and Jackson, 2007; Jackson and Hudec, 2017; Jackson and Talbot, 1986). We refer to megaflap as “packages of deep MB strata that extend far up the sides of diapirs. They are near-vertical but may also be completely overturned in their upper parts, at the transition between feeder diapirs and salt sheets” (Rowan et al., 2014).

These thickness changes and the observed stratal geometries are interpreted as reflecting salt tectonic activity accompanying salt evacuation and salt diapir rise/inflation (i.e. salt thickening by internal flow) during sedimentation. The detailed effect of syn-sedimentary salt movement during the evolution and development of the MBs is discussed based on (i) the Cotiella salt structures, (ii) stratal geometry and stratigraphic thickness variations related to halokinesis, and (iii) the distribution of the facies associations.

6.1. The Cotiella Basin salt structures

In this section, we aim at naming and describing the salt structures bounding the Armeña, Cotiella and Mediodía MBs (Figs. 2, 5A). These salt structures were interpreted as corresponding to salt walls

genetically linked spatially and temporally with gravity-driven extensional growth faulting (Brun and Fort, 2011; Fort et al., 2004; Lopez-Mir et al., 2016b, 2015). Between the Mediodía and Armeña MBs, thick Keuper evaporites are still preserved. The NW-SE elongated map pattern (Fig. 2B) of the Keuper evaporites over a distance of at least 2.5 km is consistent with the salt walls structures. We suggest the name "Mediodía salt wall" (Fig. 2B) for this salt structure. At the bottom of the Armeña MB sedimentary succession, the Keuper evaporites are cross-cutting the pre-kinematic strata and the S1 halokinetic strata which exhibits large-scale thickening wedge towards the welded Armeña salt wall (Fig. 2B, C).. This anomalous contact agrees with the growing of a salt structure during the deposition of the halokinetic strata.

The Armeña and Cotiella MBs strata are separated by a welded salt structure (Fig. 2B) as it is testified by (a) isolated outcrop of Keuper along the contact (Lopez-Mir, 2013), (b) salt-structure detritus (i.e. bi-pyramidal quartz from Keuper evaporites) reworked within the sediments forming the salt structure flanking syn-halokinetic strata and indicating Keuper exposures during their deposition, and (c) small-scale structures (detailed later) resembling to halokinetic sequences developed along passive diapirs. The map pattern of the welded salt structure striking ~NW-SE over a distance of at least 6km long (Fig. 2B), subparallel to the "Mediodía salt wall", is therefore consistent with another salt wall structure. In this paper, this salt structure is named the "welded Armeña salt wall" (Fig. 2B).

The southern border of the Cotiella MB is bounded today by another ~NW-SE striking structure: the Cotiella thrust which is interpreted as a partially inverted Cotiella extensional fault (Lopez-Mir et al., 2016b, 2015), subsequently tilted and folded by the emplacement of lower basement-involved thrust sheets (Figs. 1B, 2C). This structure is characterized by large-scale syn-halokinetic growth strata similar to those observed towards the Mediodía and Armeña salt walls (Lopez-Mir et al., 2015). Thus, it suggests that the Cotiella extensional fault was also linked to a salt wall (Lopez-Mir et al., 2015) defined as the "Cotiella salt wall" (Fig. 2B).

6.2. Regional thickness variations related to halokinesis

Unit 1 displays some marked thickness variations between the Mediodía, Armeña and Cotiella MBs. In the Mediodía MB, we assume that the exposed strata (Fig. 2B) belong to the S1 depositional sequence. The S2 sequence boundary was not observed that suggests the partial preservation of the Unit 1 and the absence of the Maciños Fm, contrarily to the Lopez-Mir et al. (2016) mapping. Therefore, even if the Unit 1 is only partially preserved, the depocenter is located in the Mediodía MB as the estimated maximum thickness is 660 m (Maciños and Angon Fms *sensu* Lopez-Mir, 2013). The Unit 1 thickness decreases progressively southward. In the Armeña MB, the Unit 1 thickness varies from ~650 m along the welded Armeña salt wall, to ~450 m in the MB center, over a distance of ~0.6 to 1.2 km (A1 and A2 sections respectively, Fig. 2B). In the Cotiella MB, the Unit 1 show minor stratal thickness variation: 150 m along the welded Armeña salt wall and 95 m downdip, over a distance of ~0.9 km (C1 and C4 sections respectively, Fig. 2B). Unit 1 thickness variations within and between MBs reflect the salt controlled initial distribution of depocenters, showing higher creation of subsidence to the North.

Unit 2 displays thickness variations between and within the Mediodía, Armeña and Cotiella MBs. Unit 2 is fully preserved in the Cotiella MB, especially along the northern margin of the MB where Unit 2 is well exposed. To the south of the MB, the thickness variation present uncertainties (Fig. 2C). The Unit 2 is not preserved in the Mediodía MB and partially preserved in the Armeña MB. Intra MBs thickness variations are expressed by important thickening or thinning toward the MB borders. The depocenter is located in the Armeña MB, suggesting a southward-directed depocenter migration since the Unit 1. There the thickness varies from ~680 m along the welded Armeña salt wall, to ~570 m in the MB center, over a distance of

~0.5 to 1 km (A1 and A2 sections respectively, Fig. 2B). To the north, in the Mediodía MB, the Unit 2 was not observed as the succession was not fully preserved. To the south, in the Cotiella MB, the Unit 2 show stratal thinning towards the welded Armeña salt wall, varying from 215 m along the welded Armeña salt wall to 305 m downdip (C1 and C4 sections respectively, Fig. 2B). The anisopachous character between the Armeña and Cotiella MBs indicates that salt-controlled subsidence was higher in the Armeña MB.

Unit 3 records a drastic change of the stratal thickness trend. The depocenter is located in the Cotiella MB, where the minimum thickness was estimated at 1.5 km. However, Unit 3 was not observed in the Armeña and Mediodía MBs. The total non-preservation of the Unit 3 in the Armeña and Mediodía MBs, is suspicious and might suggest an initial major thickness contrast. Thus, we assume that Unit 3 marked a southward brutal shift of the depocenter, downdip to the Cotiella MB northern margin, indicating a major increase of salt withdrawal in the Cotiella MB.

6.3. Stratal geometries related to halokinesis

The Mediodía MB: The Mediodía MB is 3.5 km long and 1.2 km wide (Fig. 2B). Conformably above the pre-kinematic isopachous succession, the ~0.6 km thick syn-halokinetic strata (Units 1) are not well-exposed (Fig. 5A) but might exhibit a large-scale thickening wedge towards the Mediodía salt wall, based on drone imagery (i.e. dipping towards SW, Fig. 7A).

The Armeña MB: The Armeña MB is 4 km long and 2 km wide (Fig. 2B). Conformably above the pre-kinematic isopachous succession, the ~1.5 km thick syn-halokinetic strata (Units 1, 2, 3) display a large-scale thickening wedge towards the welded Armeña salt wall (i.e. dipping towards SW, Fig. 7A).

Additionally, two smaller wedges were observed along the edge of the welded Armeña salt wall: (i) the middle part of the Unit 1 (i.e. S2 TST strata) display a syncline geometry and low-angle toplaps, compatible with a wedge-type geometry (Fig. 7B), (ii) the middle part of the Unit 2 (i.e. S3 TST strata) is thinning rapidly towards the weld, over a distance of ~300m, that is in agreement with a wedge geometry (Fig. 7C). The scale of these wedges geometries flanking the welded Armeña salt wall (Fig. 7A, B, C) is similar to that of classic wedge-type halokinetic sequences (*sensu* Gannaway et al., 2014; Giles and Lawton, 2002; Giles and Rowan, 2012; Kernen et al., 2012; Rowan et al., 2003). However, they are not capped by unconformities, and they are isolated as the stratal pattern of the Armeña MB along the edge of the welded Armeña salt wall is dominated by straight geometrical relationship (Fig. 7A, B). Nevertheless, their position along the salt structure edge reveals that they were most probably formed in response to halokinetic activity similarly to halokinetic sequences.

The landward-dipping large-scale thickening wedge displayed by the syn-halokinetic strata of the Armeña MB, as well as the occurrence of smaller scale halokinetic geometries (i.e. wedges) along the welded Armeña salt wall flanking strata, suggest extensional rollover MB coeval to salt withdrawal. Similar MBs were described in Lower Congo and Kwanza basins (Fort et al., 2004).

The Cotiella MB: The 4 km wide and 15 km long Cotiella MB is striking ~NW-SE. Along its SW border, the Cotiella MB is characterized by a ~130° striking anticline with 60–90° steeply dipping layers along the partially inverted extensional Cotiella fault (Fig. 2C). This structure exhibits a thick Unit 3 strata that thickens towards the partially inverted Cotiella extensional fault (Lopez-Mir et al., 2016b, 2016a, 2015). The underlying units are not exposed along the SW border of the Cotiella MB. Towards the center of the MB (to the NE), the northern limb anticline exhibits a long panel of flat-lying strata involving the Unit 3

strata. The overall pattern of the NE margin of the Cotiella MB is drastically different from the SW border and displays a completely overturned pre-kinematic to syn-kinematic succession (Figs. 2C, 7A) striking ~N120°. From SE to NW, the strata exhibit along-strike structural changes. In order to ease the description of these features we identify two structural domains that, from east to west, are named the Reduno and Piedra Blanca (Fig. 7A).

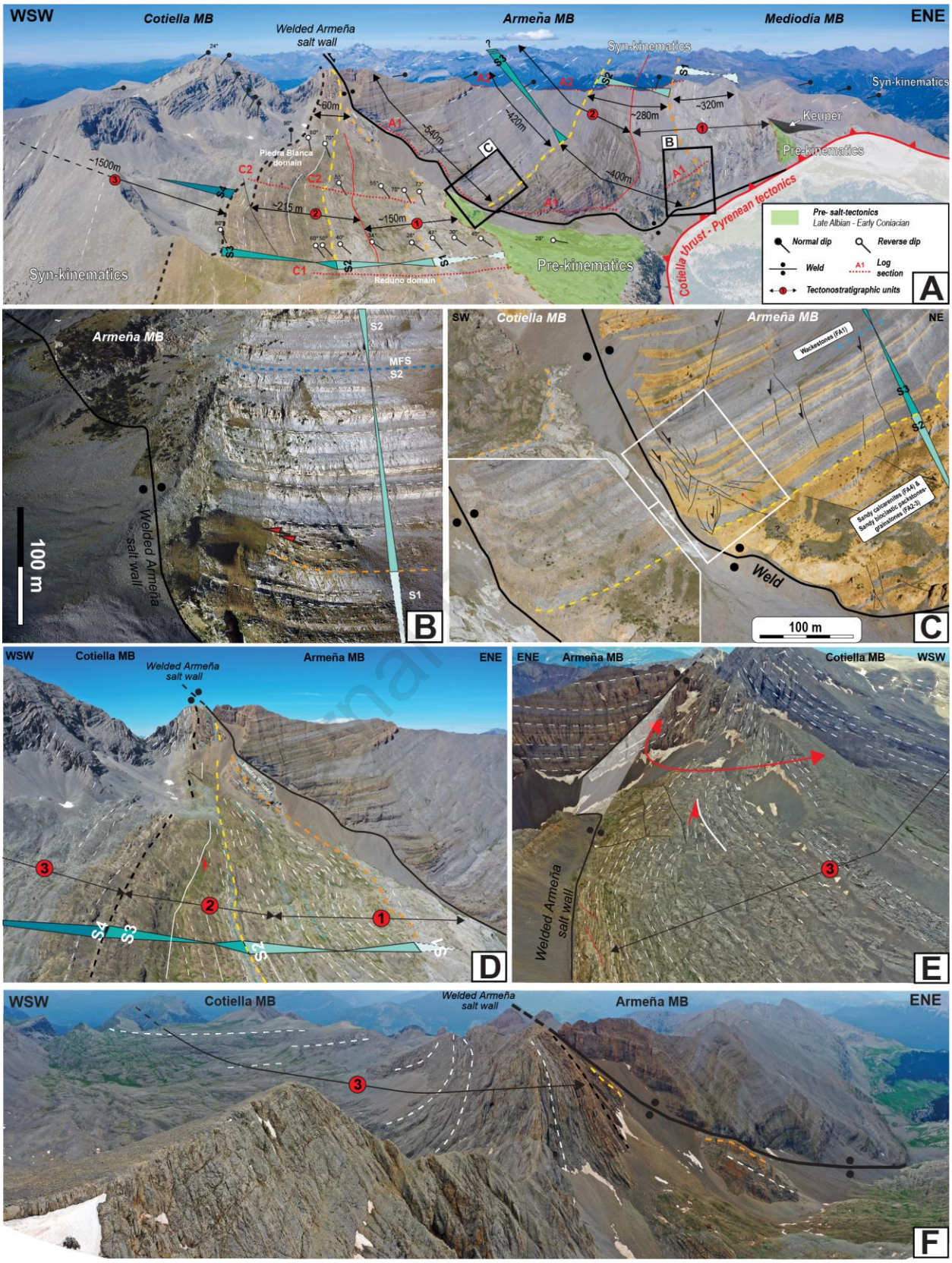
WSW
Cotiella MB
Welded Armeña salt wall
Armeña MB
Mediodía MB
ENE
Syn-kinematics
Keuper
Pre-kinematics
Piedra Blanca domain
Bielsa domain
Cotiella thrust - Pyrenean tectonics
Pre- salt-tectonics
Late Albian - Early Coniacian
Normal dip
Reverse dip
Weld
Log section
Tectonostratigraphic units
A
B
C
D
E
F
100 m
SW
NE
Wackestones (FA1)
Sandy calcarenites (FA4) & Sandy bioclastic packstones-grainstones (FA2-3)
MFS

Figure 7*: Drone pictures of the upper Coniacian-lower Santonian strata of the Cotiella and Armeña MBs. Brown dashed line= S1 Sequence Boundary (SB); Orange dashed line= S2 SB; Yellow dashed line= S3 SB; Dark dashed line= S4 SB; Blue dashed lines= MFS; Thin white dashed lines = Bedding; Thin black lines = faults; Red line = Bi-pyramidal quartz rich marker level; White line and red arrow= Internal unconformities. Localizations of viewpoints in Fig. 2B. (A) View toward the NNW of the sedimentary filling (depositional sequences and timelines) and large-scale geometries of the Cotiella and Armeña MBs. Locations of the logged stratigraphic sections (see Fig. 2B for localization in map view) and close-up views (B, C). (B) The small-scale wedge geometry included within Unit 1 strata of the Armeña MB. (C) The small-scale wedge geometry included within Unit 2 strata of the Armeña MB. (D) View toward the NNW of the large-scale thinning wedge towards the weld of the units 1 and 2 strata of the Cotiella MB; (E-F) View toward the SSE (E) and NNW (F) of the large-scale thinning wedge towards the weld of the Cotiella MB Unit 3 strata.*

In the Piedra Blanca and Reduno domains (Fig. 7A), the pre-kinematic successions exhibit strongly overturned pre-kinematic strata (with beds inclined less than 25°) from upper Cenomanian to lower Coniacian (Fig. 7A). However, structural changes are frequent because Cenozoic normal faults dipping towards ~NE affect the NE border of the Cotiella MB. These normal faults are also affecting the lower part of the Unit 1 (i.e. S1 sequence, Fig. 7A) of the Cotiella MB and involves complex dip evolution, making the identification of potential wedging hazardous. On the contrary, the uppermost strata of the Unit 1 (i.e. S2 sequence) sedimentary layers forms a spectacular wedge thinning toward the welded Armeña salt wall (towards NE, Fig. 7A), and finally truncated to the top by the Unit 2 (i.e. S3 sequence, Fig. 7A). This large-scale geometry flanking the salt structure edge bounded at the top by an unconformity indicates a salt-controlled development.

The Unit 2 is also characterized by wedge thinning toward the welded Armeña salt wall (towards NE, Fig. 7A, D) characterized by dip evolution from 60° lowermost to 80° uppermost Unit 2 strata in the Reduno domain, from 70 to 90° overturned strata in the Piedra Blanca domain (Fig. 7A) and from 60 to 75° overturned strata in the Lavasar valley (section C3, Fig. 2B). The Unit 2 sedimentary layers also exhibits an internal truncation (red line, Fig. 7A, D) characterized by low angle toplaps, that was formed before the ~70-90° tilting recorded during Unit 3. Actually, the overall pattern of deposition of the Unit 3 exhibits a spectacular wedge thinning towards the welded Armeña salt wall and characterized by beds dips which range from vertical along the margins to less than 30° in the center of the MB (Fig. 7A, E, F). Internal unconformities characterized by low angle toplaps towards the welded Armeña salt wall (Fig. 7E) suggests again wedges controlled by halokinetic activity.

Finally, the completely overturned pre-kinematic to syn-kinematic succession of the NE margin of the Cotiella MB, including salt-controlled small- (Units 1 and 2) and large-scale (Unit 3) wedges suggest a megaflap structure (*sensu* Callot et al., 2016; Rowan et al., 2016).

6.4 Distribution of facies associations

The relative proportion of facies association recorded vertically and laterally within each MB vary not only from proximal to distal zones as for classical mixed siliciclastic carbonate platform, but also appears locally controlled by salt-induced topography.

In this section, we will analyze in detail the relationship between the stratal pattern flanking salt structures and the distribution of facies, through the successive tectonostratigraphic units of the Armeña and Cotiella

MBs. As described previously, the Cotiella MBs are filled by a stack of 5-30 m thick parasequences, which are individually characterized by coarsening-upwards and shallowing-upwards trends of depositional conditions (Fig. 6). In order to simplify the facies classification, we suggest two main facies groups: (i) a mud-prone facies corresponding to the fine-grained wackestones (FA1), and (ii) a sand-prone facies corresponding to the sandy bioclastic packstones-grainstones (FA2, FA3) and the sandy-rich calcarenites (FA4).

The Armeña MB: Based on the spectacular NE-SW panorama of the Armeña MB and using sedimentological section A1 (close to the weld) and A2 (downdip to the welded Armeña salt wall margin), the Fig. 8 displays the vertical and lateral variations of the stratal pattern and the distribution of facies. Based on correlations between 3 stratigraphic sections of S1, S2 and S3 parasequences (A1, A2, A3 sections, Fig. 2B), the Fig. 9 shows the lateral facies distribution in 3D (fence diagram). The overall pattern of the spatial distribution of lithofacies (Figs 8 & 9) is characterized by an asymmetric stratal thickening and coarsening adjacent to the welded Armeña salt wall margin (i.e. towards SW, Fig. 2B), suggesting an elongated NW-SE trending belt of more sand-prone facies along the welded Armeña salt wall.

Unit 1: Only the uppermost deposits of the unit 1 were logged and exhibit type 1 carbonate-dominated parasequences (Fig. 6). Medium to coarse grained inner to middle ramp facies (FA2, FA3) are localized along the welded Armeña salt wall and pass laterally and downdip to fine to medium-grained middle ramp sediments (FA2; Fig. 9). These facies transitions are gradual (over a distance of ~0.9-1.4 km) and exhibit sheet-like layers, with rare lateral pinch outs into outer ramp fine-grained wackestones (FA1; Fig. 9). The percentage of sandy bioclastic packstones-grainstones (FA2, FA3) is relatively homogeneous and varies from ~40% along the welded Armeña salt wall to ~30-35% in the MB center (sections A1 and A2 respectively, Fig. 9).

Unit 2: The Unit 2 marks an abrupt increase of the sand-prone facies (i.e. ~80% along the welded Armeña salt wall margin, vs 65-40% downdip; Fig. 9). This transition results from the appearance of type 2 terrigenous-dominated parasequences (Fig. 6), characterized by medium to very coarse-grained cross-bedded sandy-dominated inner to middle ramp facies (FA4) along the welded Armeña salt wall and passing laterally towards the MB center to fine to medium grained middle ramp sediments (FA2 and FA4) (sections A1 and A2/A3 respectively, Fig. 9). Internally to the Unit 2, brutal change of the stratal pattern and the facies distribution trends occurs in the Armeña MB. The Unit 2 can be subdivided into 3 sub-units:

Sub-Unit 2a: The facies transitions are gradual along sheet like layers fining and thinning towards the MB center (i) over distances of at least ~0.9-1.2 km (Figs. 8, 9), or (ii) over distance of ~600m with rapid lateral pinch out into outer ramp fine-grained wackestones deposits (FA1, Figs. 9 & 10).

Sub-Unit 2b*:* The facies distribution trend exhibits very rapid facies changes characterized by medium to coarse grained sand-prone inner to middle ramp facies (FA2, FA3 and FA4) along the welded Armeña salt wall and passing laterally to fine-grained wackestones facies (FA1) (sections A1 and A2/A3 respectively, Fig. 9). This facies transition is abrupt and occurs over distances of ~200-400 m, exhibiting laterally discontinuous sheet like layers fining and thinning towards the MB center. The sand-prone facies ratio (FA2, 3, 4) varies from ~50% along the welded Armeña salt wall to 0-10% in the MB center (sections A1 and A2/A3 respectively, Fig. 9).

Sub-Unit 2c: The transition between Unit 2b and Unit 2c is sharp and corresponds to a brutal progradation of sand-prone facies towards the MB center. The facies distribution is characterized by sheet-like sand-prone sediments (FA2, FA3, FA4) representing a percentage evolving from 80% along the welded Armeña salt wall to 70% towards the MB center, over a distance of about ~300 to 600 m (Fig. 9). This facies

distribution homogeneity matches well with the relatively uniform stratal thickness and the minor wedging geometry.

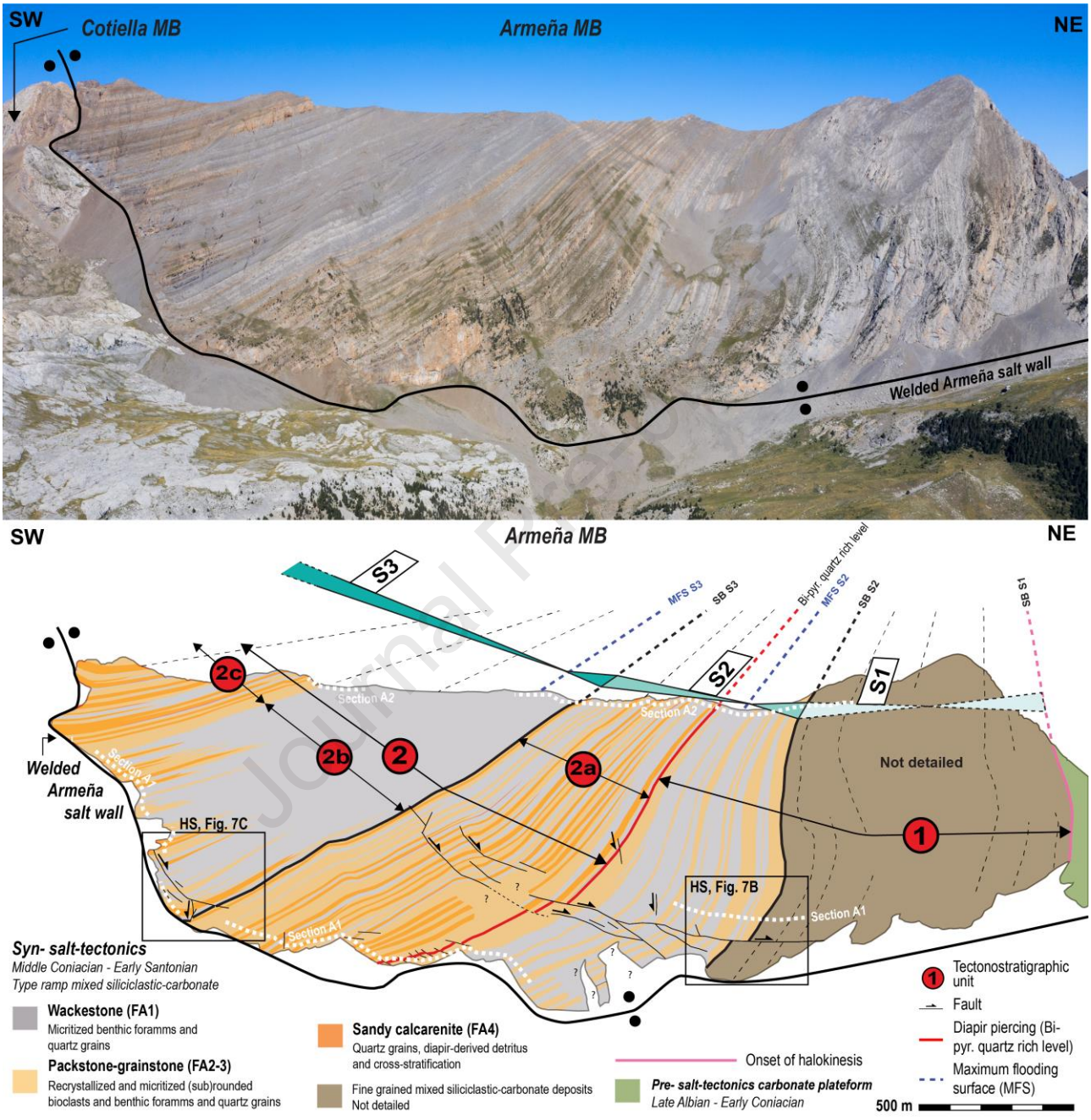

***Figure 8**: NE-SW panorama of the Armeña MB showing the facies distribution inside each tectonostratigraphic unit. The interpretation was performed based on sections A1, along the Armeña salt wall, and A2, along the Armeña crest (Fig. 2B), and drone imagery.*

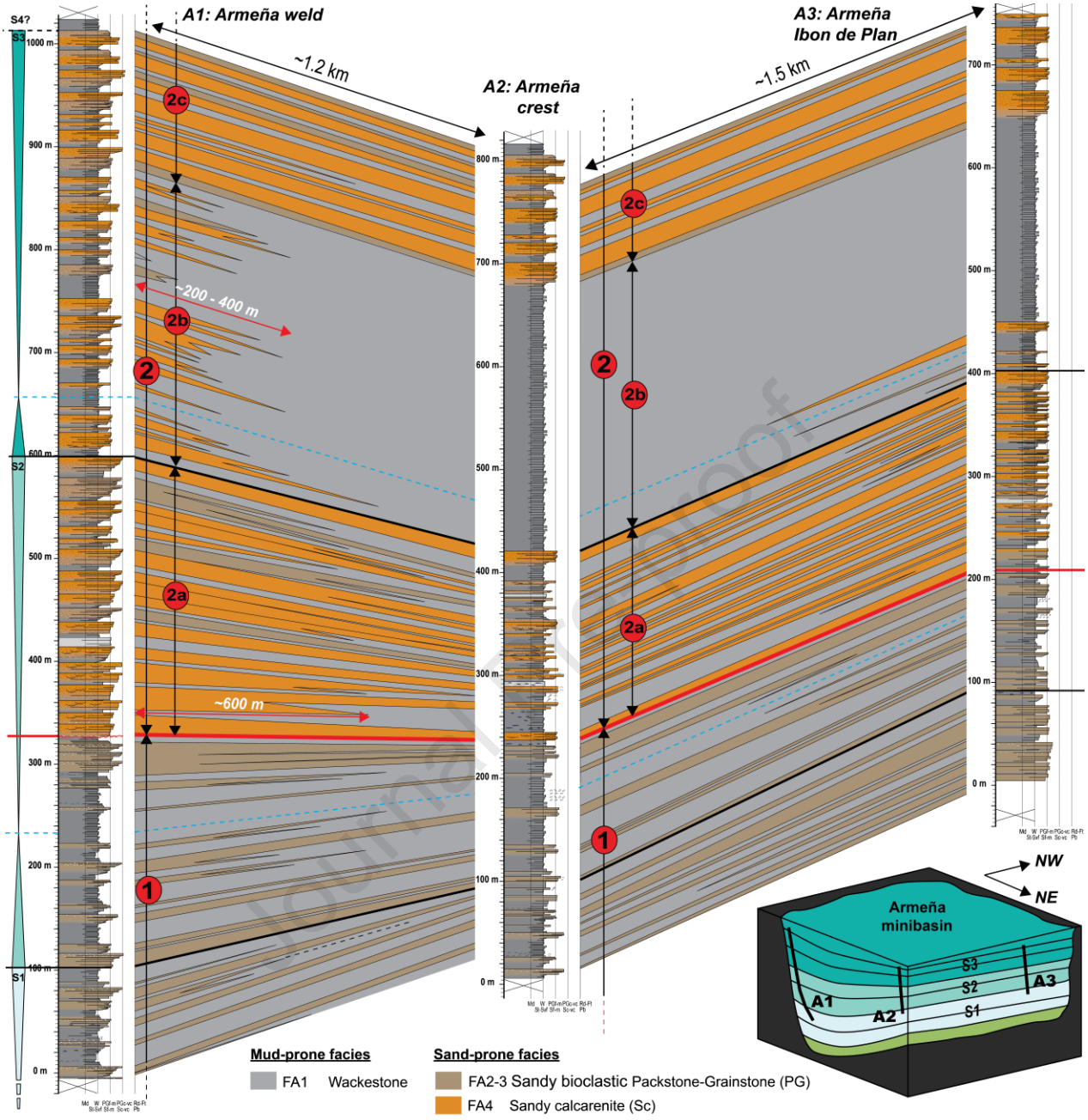

Sand-to-Wackestone %					
	A1 Armeña weld	1 305 m thick min. 40% PG 60% Wackestone	2	2a 270 m 80% Sc + PG 20% Wackestone	2b 280 m 50% Sc + PG 50% Wackestone	2c 132 m thick min. 80% Sc + PG 20% Wackestone
	A2 Armeña crest	1 233 m thick min. 30% PG 70% Wackestone	2	2a 185 m 40% Sc +PG 60% Wackestone	2b 260 m 0% Sc + PG 100% Wackestone	2c 125 m thick min. 70% Sc + PG 30% Wackestone
	A3 Armeña Ibon de Plan	1 210 m thick min. 35% PG 65% Wackestone	2	2a 190 m 65% Sc + PG 35% Wackestone	2b 245 m 10% Sc + PG (FA2-3-4) 90% Wackestone	2c 100 m thick min. 70% Sc + PG 30% Wackestone

***Figure 9**: Stratigraphic fence diagram of the syn-halokinetic upper Coniacian-lower Santonian strata of the Armeña MB illustrating the distribution and the ratio of mud and sand, the stratal pattern and the relative thickness within each tectonostratigraphic unit from the welded Armeña salt wall margin (sections*

A1 and A2) towards the MB center (sections A2 and A3). Localization of stratigraphic sections in map in Fig. 2B.

The Cotiella MB: Based on the spectacular panorama exhibiting a dip and strike view (Fig. 7A) and using sedimentological section C1 (Reduno) and C2 (Piedra Blanca), the Fig. 10 illustrates (i) an along strike facies distribution of sand-prone facies of parasequences along the welded Armeña salt wall, and (ii) basin-wide timeline correlations in 3D using C3 and C4 cross-sections located at the western border of the Cotiella massif (Fig. 2B). The overall pattern of the spatial distribution of lithofacies is characterized by an asymmetric stratal thinning and coarsening adjacent to the welded Armeña salt wall (Fig. 10) and by shallower and coarser lithofacies towards the SE (sections C1 and C2).

Unit 1: This unit is characterized by strong thickness variations. The minimum thickness of 32 m was recorded at the Lavazar section while the maximum thickness of 116 m was recorded at the Piedra Blanca section (sections C3 and C2, respectively, Fig. 10). This thickness variation might be involved by a local depocenter controlled by salt withdrawal associated to abrupt stratal thickening towards the welded Armeña salt wall margin (Fig. 7D). The ratio of sandy bioclastic packstones-grainstones (FA2, FA3) shows a minor increase from ~55% and 40% along the welded Armeña salt wall margin to ~60% downdip (respectively C1/C2 and C4 sections, Fig. 10).

Unit 2: As for the Armeña MB, Unit 2 marks an abrupt increase of the sandy-rich facies proportion. In the Cotiella MB, unit 2 exhibits an overall pattern of laterally continuous sheet like layers with lateral thickness changes (Fig. 10). Along the welded Armeña salt wall margin (sections C1, C2, C3), the Unit 2 is 180-215m thick and is characterized by a ~70-75% homogeneous ratio of sandy-rich facies (sections C1 and C2, Fig. 10) made of medium to very-coarse grained inner to middle ramp facies (FA3, FA4). Towards the MB center, downdip to the welded Armeña salt wall margin (section C4, Fig. 10), Unit 2 strata (i) is thicker (304 m), (ii) exhibit lowest ratio of sandy-rich facies (60%) and (iii) finer grained middle ramp sediments (FA2, FA4) (Fig. 10). These spatial variations of thickness and facies agree with the overall stratal pattern of the Unit 2, forming a large-scale wedge thinning towards the welded Armeña salt wall (Figs. 7A, 8D).

Unit 3: This Unit 3 marks a brutal change in the facies assemblage of the succession, from underlying sand-rich dominated units (i.e. ~50-70% of sandy rich facies) to a fine-grained wackestones dominated unit (i.e. ~0-10% of sandy rich facies) (Fig. 10).

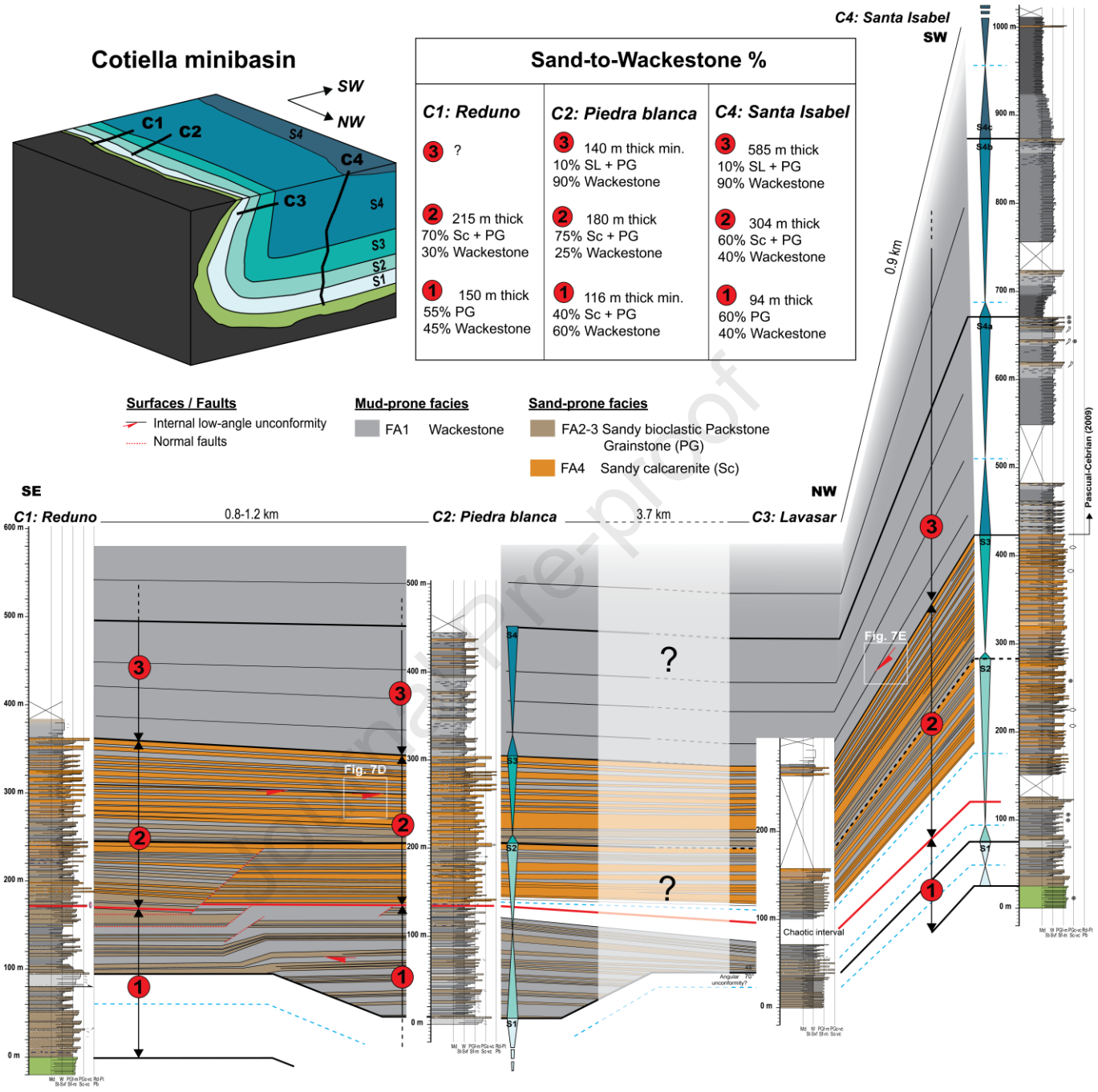

***Figure 10**: Stratigraphic fence diagram of the syn-halokinetic upper Coniacian-lower Santonian strata of the Cotiella MB showing the distribution and the ratio of sandy-rich facies, stratal pattern and relative thickness within each tectonostratigraphic unit along the welded Armeña salt wall margin (C1, C2 and C3 sections) and downdip (C3 and C4 sections). Localization of sections in Fig. 2B.*

7. Paleogeographic tectonostratigraphic reconstruction

In order to discuss the impact of halokinesis accompanying salt withdrawal and diapirism on the sedimentation, Fig. 11 proposes a tectonostratigraphic evolution of the Cotiella MBs by combining stratal pattern evolutions, halokinetic geometries, stratigraphic thickness variations and the distribution of facies assemblages.

Regional lithofacies trends combined with thickness trends suggest that sand deposited in a proximal-distal profile oriented ~N-S. The progressive north to northeastward deepening of facies and associated decrease in sandy-rich facies proportion support a north to northeast-dipping slope and ~east to west–oriented shoreline, as it is commonly proposed in the literature (e.g., Andrieu et al., 2021; Martín-Chivelet et al., 2019). Detrital sand (type 1) was likely transported from highlands to the S (Ebro massif) towards the shoreline to the N, by river and deltaic systems, where it was reworked and redistributed by wave and tidal current processes (Lopez-Mir, 2013).

However, salt can form topographically elevated walls or diapirs that impose a strong local control on sediment dispersal and the resulting facies distributions (Banham and Mountney, 2013; Ribes et al., 2015). In this section, we aim at analyzing the impact of the growing welded Armeña salt wall on facies distribution, stratal pattern, and thickness trends. By combining the vertical evolution of stratal geometries, the regional isopach pattern and the facies distribution, we have subdivided the development of the welded welded Armeña salt wall into 4 main tectonostratigraphic phases (Figs. 11, 12).

Initiation of salt inflation: Unit 1

During Unit 1, the maximum thickness of ~600m was recorded to the North, along the Mediodía MB while to the south, in the Cotiella MB, very minor thickness changes (~100-150 m) were recorded indicating higher rates of salt inflation (i.e. salt thickening by internal flow) towards North. This is in accordance with the overall pattern of km-scale landward facing growth-strata, both in the Armeña and Mediodía MBs (Fig. 11). These geometries facing the continent (i.e. toward South), recorded during post-rift period, are compatible with an initiation of extensional rollover MBs coeval to salt withdrawal. In the Armeña MB, straight geometrical relationships towards the welded Armeña salt wall are dominant and one small-scale wedge was recorded (Figs. 7B, 8). Consequently, this small-scale salt-structure indicate that the ratio between diapir-rise rate and sediment-accumulation rate increase episodically.

During Unit 1, first mixed siliciclastic-carbonate sedimentation took place. The main impact of halokinesis on facies distribution is recorded by thickness variation between the Armeña MB and the Cotiella MB, as well as the average thickness of individual parasequences (i.e. ~5-10 m in the Cotiella MB vs 10-30 m in the Armeña MB, Figs. 9, 10, 12). The uppermost shallow water and coarse-grained facies of individual parasequences are: (i) spatially organized as sheet-like layers laterally continuous over >1 km; (ii) gradually thinning and fining towards the salt walls (Fig. 11). In the Cotiella MB, they are commonly coarse grained (i.e. FA3 middle to inner ramp environment, Fig. 3D, E). In the Armeña MB, these FA3 coarse-grained deposits are located along the welded Armeña salt wall margin (section A1) and exhibit gradual finning and thinning towards the MB center (i.e. section A2, Fig. 2B), with rare lateral pinch-outs into FA1 outer ramp fine-grained wackestones. The proportion of sandy-rich facies varies from 45 % in the Cotiella MB to 30% in the northernmost section of the Armeña MB (sections C1 and A2, respectively; Fig. 12). This progressive finning of facies towards ~N agrees with the basin paleogeography implying ~S-N direction of sediment supply. The overall pattern of sheet-like sedimentary layers, characterized by progressive facies transitions over distances of kms, suggests minor impact of salt topography on sedimentation and probably

high sedimentation rates, indicating that salt structures were still capped by sediments. However, small topographies inflated by salt structure rise might be indirectly highlighted by the rudist fragments rich FA2b subfacies described along the northern border of the Cotiella MB (Fig. 3D), indicating that local rudist patch reefs developed on local paleohighs (Fig. 11).

Salt evacuation and rapid downbuilding of the Armeña MB: Unit 2.

The transition between the salt inflation observed during Unit 1 and the salt evacuation (i.e. salt extrusion on the seafloor) observed during Unit 2 is based on the recognition of (i) an increase of the amount of wedging along the welded Armeña salt wall (Fig. 12), (ii) the spatial variation of thickness trends (Figs. 11, 12), (iii) the mud/sand ratio change, and (iv) the coeval appearance of sedimentary layers rich in bi-pyramidal quartz reworked from Keuper evaporites (Fig. 3E, F), confirming that exposed salt walls were flanking the Armeña and Cotiella MBs. The depocenter located along the southern flank of the Armeña MB during Unit 2, as well as the presence of small-scale wedges in both sides of the welded Armeña salt wall (Fig. 7A, C, D), testifies that the depocenter results from downbuilding acceleration in response to the onset of salt evacuation and the increase of sedimentation load.

Along the welded Armeña salt wall flanking strata (Fig. 11), straight geometrical relationships towards the salt wall are still dominant and one small-scale wedge geometry were recorded (Figs. 7C, 8). Consequently, in the Armeña MB, the sediment-accumulation rate is higher than the salt wall rise rate, indicating that the salt-controlled during Unit 2 mainly impacted thickness trends, stratal pattern and facies distribution. In the Cotiella MB, the wedging rate increases brutally from 0-5% to 20% (Fig. 12), suggesting an acceleration of the Cotiella MB downbuilding and/or an increase of the salt flow rate. This is testified by changes in stratal pattern and facies dispersal trends (i.e. finning and thinning sheet-like layers towards the welded Armeña salt wall, Fig. 12).

During the development of Unit 2, sedimentary system and distribution of sedimentary facies were deeply impacted, evolving from carbonate dominated parasequences, exhibiting sheet like layers and progressive facies transitions over distances of kms (unit 1), to tide-dominated terrigenous parasequences (type 2 , Figs. 6, 11) exhibiting also sheet like layers but with shorter progressive facies transitions, over distances of hundreds of meters downdip to the welded Armeña salt wall (~0.6 km and ~0.2-0.4 km for sub-units 2a and 2b of the Armeña MB, respectively; Fig. 12). The dominant east to southeastward orientation of paleocurrents indicates a westerly provenance for the clastic material supplying the unit 2 strata. This is uncommon as the more distal parts of the post-rift basin are located to the North (Jammes et al., 2009; Masini et al., 2014; Roca et al., 2011; Tugend et al., 2015, 2014). This indicates that the paleocurrents are orthogonal to the northward-directed classic paleo-directions of drainage, suggesting drainage pattern was probably primary controlled by salt topographies (Fries and Parize, 2003). This is corroborated by the direction of the welded Armeña salt wall striking NW-SE, which is compatible with the E to SE paleocurrents. We propose here that the salt evacuation formed topographically elevated salt walls that amplified tidal currents along strike and facilitate the accumulation of sandy-rich facies along the salt wall margin (Figs. 11, 12).

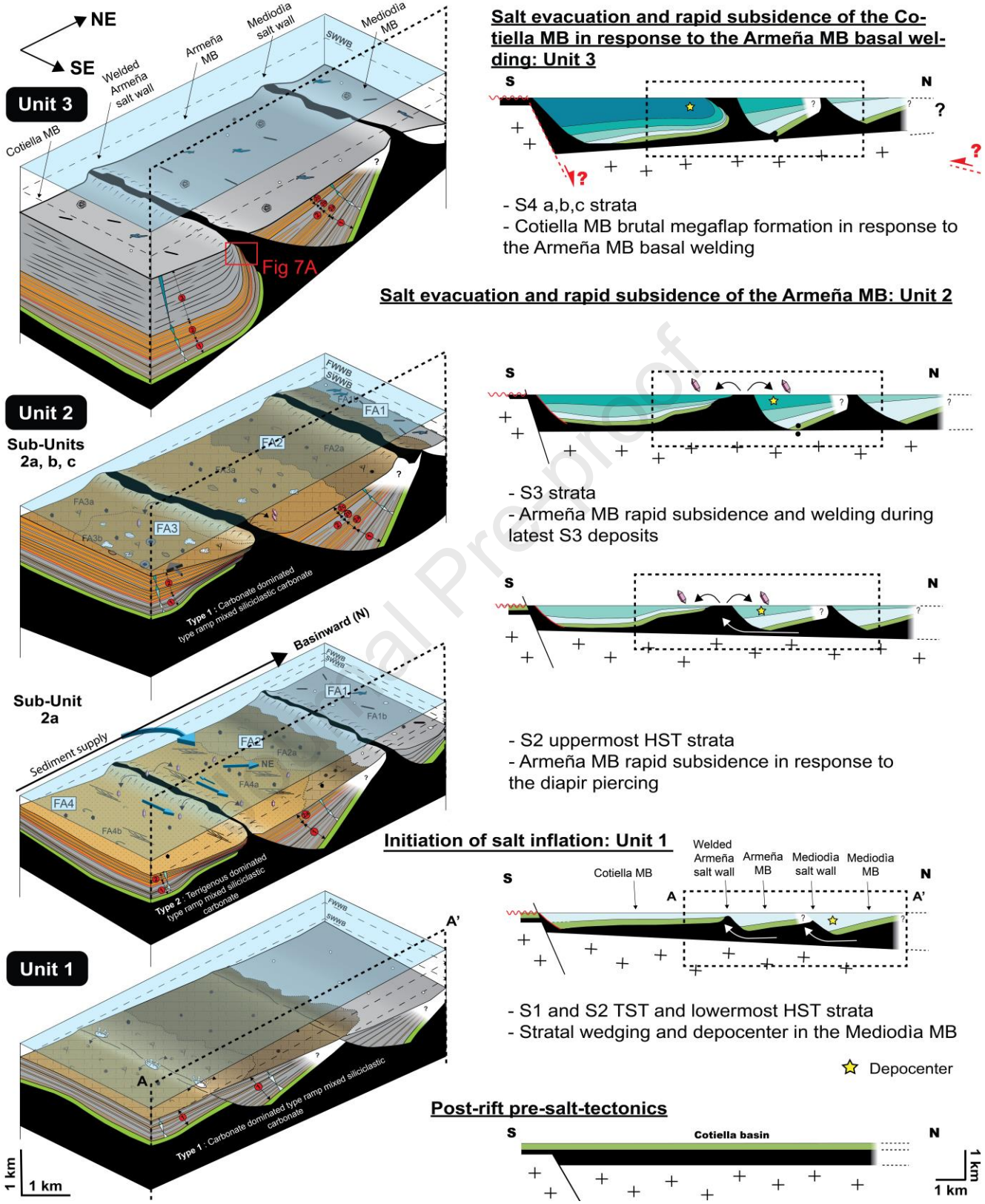

***Figure 11**: Schematic NE-SW 2D and 3D cross-section showing the Cotiella MBs tectonostratigraphic evolution of the syn-halokinetic upper Coniacian-lower Santonian strata and its relationship with the main*

sedimentary and tectonic events occurring in the Cotiella MBs. MB= MB; TS= Tectonostratigraphic unit; TST= Transgressive system tract; HST= Highstand system tract. Legend in Fig. 6.

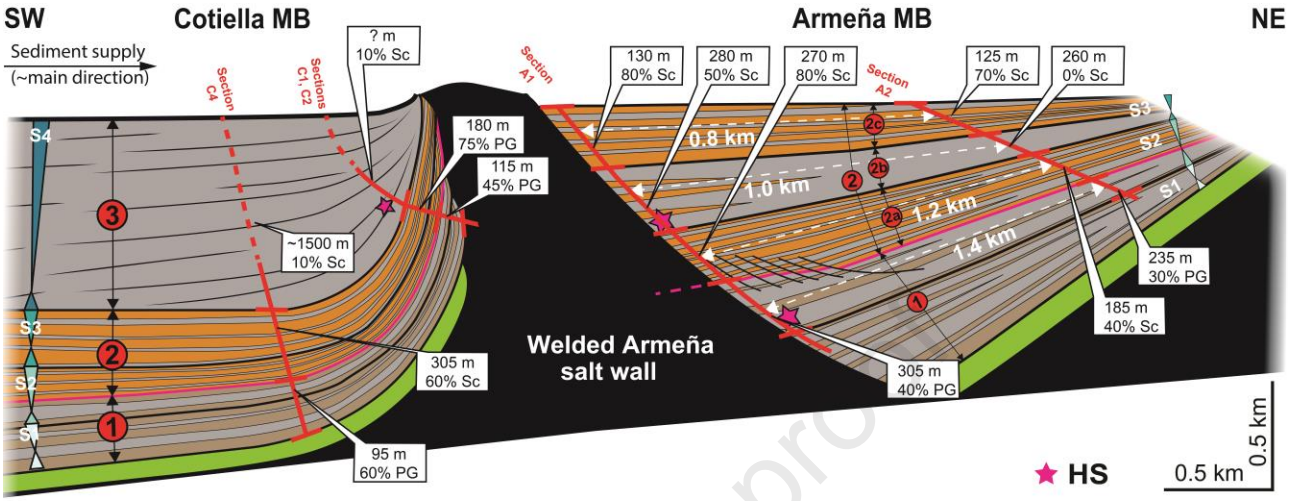

MB type	Tectono-stratigraphic unit (TS)		Halokinetic small-scale geometry (HS)	Halokinetic TS unit wedging % towards the salt wall	Facies changes in the halokinetic TS unit (Proximal → Distal)	Stratal pattern in the halokinetic TS unit	Ratio between the diapir rise rate and sedimentation rate	Topographic relief	Parasequence type & average thickness	Section	Average parasequence facies ratio (PG= Packstones Grainstones - FA2-3 (0-10 % sand); Sc= Sandy calcarenites - FA4 (20-60% sand); W= Wackestones - FA1 (0-10% sand))	
Armeña MB Extensional rollover Seismic-scale thickening wedge towards the Armeña salt wall	Unit 1 Salt inflation	1	Wedge (S2 TST)	~30 % over 1.4 km	Gradual fining and thinning seaward	Laterally continuous sheet-like layers (> 1 km)	++	+	Type 1 ~10-30 m	A1	PG=40%	W=60%
										A2	PG=30%	W=70%
	Unit 2 Salt evacuation	2a	/	~30 % over 1.2 km	Rapid finning and thinning seaward	Laterally continuous and discontinuous sheet-like layers (~0.6 km)	++	++	Type 1, 2 ~5-20 m	A1	PG + Sc =80%	W=20%
										A2	PG + Sc =40%	W=60%
		2b	Wedge (S3 TST)	~10 % over 1.0 km	Very rapid fining and thinning seaward	Laterally discontinuous sheet-like layers (~0.2-0.4 km)	++	++	Type 1, 2 ~5-20 m	A1	PG + Sc =50%	W=50%
										A2	PG + Sc =0%	W=100%
		2c	/	~5 % over 0.8 km	Gradual fining and thinning seaward	Laterally continuous sheet-like layers (> 0.8 km)	+	++	Type 1, 2 ~5-20 m	A1	PG + Sc =80%	W=20%
										A2	PG + Sc =70%	W=30%
Cotiella MB Megaflap Seismic-scale thinning wedge towards the Armeña salt wall	Unit 1 Salt inflation	1	/	~0-5 % over ~1 km	Gradual fining and thinning seaward	Laterally continuous sheet-like layers	+	+	Type 1 ~5-10 m	C1 C2	PG=45%	W=55%
										C3	PG=60%	W=40%
	Unit 2 Salt evacuation	2	Wedge (S2 TST) /	~20 % over ~1 km	Rapid finning and thinning seaward	Laterally continuous sheet-like layers	++	++	Type 1, 2 ~5-10 m	C1 C2	PG + Sc =75%	W=30%
										C3	PG + Sc =60%	W=40%
	Unit 3 Salt evacuation	3	Wedges (S4)	~60 % over ~1 km	Gradual fining and thinning seaward	Laterally continuous and discontinuous sheet-like layers	+++	+++	Type 1, 2 ~10-30 m	C1 C2 C3	PG + Sc =10%	W= 90%

***Figure 12**: Schematic SW-NE cross-section showing the syn-halokinetic upper Coniacian-lower Santonian facies distribution, stratal pattern, thickness trends and halokinetic geometries of the Armeña and Cotiella MBs and its relationships with the 3 main tectonostratigraphic units (TS) detailed in Fig. 11. The cross-section depict the average parasequence ratio in each TS. HS= halokinetic sequence; MB= Minibasin; TS= Tectonostratigraphic unit.*

Salt evacuation and rapid downbuilding of the Cotiella MB in response to the Armeña MB basal welding: Unit 3

This stage implied a southward-directed migration of the depocenter, along the northern margin of the Cotiella MB (Figs. 11, 12). There, Unit 3 strata exhibit large halokinetic growth-strata including internal low angle unconformities and suggesting syn-depositional folding of at least 70° from base to top (Fig. 7). This spectacular geometry coeval to the 1.5 km thick Unit 3 strata both suggest a major increase in salt flow (Fig. 8C) and creation of subsidence. Salt-controlled wedging, estimated at 60% over distances of 1 km, as well as small-scale wedges along the northern Cotiella MB flank, confirm that passive diapirism was dominant.

This salt-controlled event implied major changes in spatial variation of thickness trends, the stratal pattern trends and impacted sedimentary system and distribution of sedimentary facies. The ~1.5 km thick Unit 3 in the Cotiella MB (Fig. 11) contrasting with the total absence of the unit 3 in the Armeña MB, was interpreted as being, at least, an initial major thickness variation between the 2 MBs. This assumption is coherent with a brutal decrease of accommodation space creation in the Armeña and Mediodía MBs in response to the Armeña MB basal welding. The Unit 3 marks also a major transition towards fine-grained outer ramp carbonate facies involving a brutal decrease of sandy-rich facies ratio (Fig. 12), most probably controlled by basin-scale (i.e. tectonic subsidence) or global (i.e. eustatic-driven sea-level rise) allochthonous factors as discussed below.

8. Discussion

In the following sections, we evaluate the impact of allochthonous factors on halokinesis and sedimentation, including the deformation of the stratal packages near salt structures, the location of depocenters and their migration through time. We then compare our results to the published models derived from predominantly shallow-water settings in Pyrenees with Aulet and Adons diapirs (Gannaway et al., 2022; Saura et al., 2016) and deep-water settings with the Bakio Diapir (Poprawski et al., 2016, 2014; Roca et al., 2021).

8.1. Allochthonous factors controlling sedimentation

During the late Coniacian-early Santonian, the region is in a post-rift context (Martín-Chivelet et al., 2019). Tectonic quiescence, thermal subsidence, and eustatic sea-level changes were driving sea-level fluctuations as it is testified by consistent thicknesses and lithologies throughout the South Pyrenean Basin (Martín-Chivelet et al., 2019). However, the Ribagorçana and Cotiella basins (Fig. 1A) as an exception are displaying rapid changes in thickness and lithology interpreted in response to halokinesis (Gannaway et al., 2022; García Senz, 2002; Lopez-Mir, 2013; Saura et al., 2016; Souquet, 1984, 1967).

The late Coniacian-early Santonian interval corresponds to a 4-5 My time interval. Despite the lack of time control, we tentatively suggest a ~1 to 3 Ma time duration of individual depositional sequences. In this scenario, this is compatible with 3rd order depositional sequences, commonly attributed to global eustatic sea-level fluctuations (Haq et al., 1988). This agrees with the individual depositional sequences internally organized as stacked parasequences, which are classically attributed to high-frequency eustatic sea-level variations in response to climatic perturbations related to Milankovitch cycles. In this scenario, eustatic-driven floodings of the late Coniacian-early Santonian (KCo2, KSa1 and KSa2, Haq, 2014) might be recorded in the Cotiella MBs by the MFS of the stratigraphic succession (Fig. 2A) displaying criteria for basin-wide major basinward facies shift: (i) the S2 MFS (~KCo2?) is characterized by *Lacazina elongata*

and calcisphere-rich marker level; (ii) the S3 MFS (~ KSa1?) is characterized by a richness in silicified spicules and cherts; (iii) The S4 depositional sequence (S4 MFS ~ KSa2?) marks a major depositional shift, characterized by a richness in cherts and silicified sponge spicules within outer ramp fine-grained deposits. Moreover, this unit displays a regional extension (Gannaway et al., 2022; García Senz, 2002).

The onset of salt-evacuation marks the transition between Unit 1 and Unit 2 (i.e. Figs. 11, 12) which corresponds to an intra-S2 depositional sequence marker level. This transition displays (i) major change of salt-induced accommodation and wedging rates in the Cotiella MBs (Fig. 12), and (ii) an abrupt increase of siliciclastic fraction (i.e. terrigenous dominated type 2 parasequences, Fig. 12). This major change in the siliciclastic ratio implies new sedimentary inputs from hinterlands (i.e. Ebro massif?). The perfect coincidence between the onset of salt-evacuation and the abrupt appearance of sandy-dominated facies might indicate a basin-scale event impacting (i) drainage system in proximal areas (i.e. uplift of the hinterland, barrier destruction) and (ii) halokinesis. This basin-scale event might be in response to the collapse of the post-rift platforms triggered by the late stages of the northern Iberian margin progressive tilting toward the north related to post-rift thermal subsidence (Lopez-Mir et al., 2015; McClay et al., 2004).

According to the Haq (2014) eustatic curve, the sea-level rises of the KSa1, KCo2 and KSa2 were relatively equivalent (~+210 m). However, in the Cotiella MB, the sedimentary response of the S4 depositional sequence (~KSa2 ?) is very different from the S1 and S3 depositional sequences (~KCo2 and KSa1 respectively). The S4 depositional sequence (~Aguasalenz Fm) displays a regional major deepening phase, as the Aguasalenz Fm and the equivalent Anserola Marls have a regional extension within the Cotiella-Boixols thrust sheet and exhibit relatively homogeneous deepwater facies (Gannaway et al., 2022; García Senz, 2002). Altogether, it suggests that the S4 eustatic-driven basinward shift of facies invoke tectonic subsidence as additional factors. This is in accordance with the perfect coincidence between the onset of Aguasalenz Fm (S4 depositional sequence, Fig. 12) and the onset of the Unit 3 in the Cotiella MBs (i.e. brutal downbuilding of the Cotiella MB in response to the basal welding of the Armeña MB, Figs. 11, 12), suggesting that onset of salt-controlled unit 3 (Fig. 11) might have been (partly?) involved by a basin-scale tectonic event. This basin-scale event might be in response to another event during the collapse of the post-rift successions related to post-rift thermal subsidence (Lopez-Mir et al., 2015; McClay et al., 2004). Another possibility could be the onset of Pyrenean orogeny earlier than generally proposed. The onset of Pyrenean compression is generally interpreted as being middle Santonian in age and coeval to the Campos Breccia appearance, which is overlying the Unit 3 (Fig. 2A, B, C). The onset of Unit 3 marks a rapid southward directed migration of the depocenter coeval to the onset of a large-scale southward directed 90° thickening wedge geometry, which are both compatible with the southward directed tilting of the Cotiella Basin in response to the Pyrenean compression (Fig. 11). In this proposition, the onset of the Pyrenean orogeny would be time equivalent to the onset of the Unit 3 (Fig. 11).

These assumptions indicate that tectono-sedimentary unit transitions seem to be also controlled by allochthonous factors, impacting the halokinetic activity within the Cotiella Basin, and by consequence, sedimentary systems and their relative distribution of sedimentary facies.

8.2. Comparison with other Pyrenean MBs

In the previous section, we discussed the impact of the halokinesis on the mixed siliciclastic-carbonate facies distribution of eustatic-driven depositional sequences. In this section, we aim at comparing our results with integrated field-based tectono-sedimentary studies on other examples from the Pyrenees, characterized by different salt structures and sedimentary systems: the Ribagorcana MBs (Gannaway et al., 2022; Saura et al., 2016) and the Bakio diapir (Poprawski et al., 2016, 2014; Roca et al., 2021).

8.2.1 The Ribagorçana Minibasins

The Ribagorçana Basin is located in the south-central Pyrenees (Fig. 1C) and displays three MBs (Sopeira, Faiada and Sant Gervàs) and two diapirs (Aulet and Adons). There, the upper Albian to Santonian synrift to postrift strata recorded additional influence of passive diapirism and salt evacuation in response to gravity-driven extension above the Keuper evaporites (Gannaway et al., 2022). Sedimentary systems are characterized by carbonate platform deposits evolving from a wave-dominated shoreface on a gentle ramp (Aulet Formation, late Albian-early Cenomanian) to a deepening basin with a steep, rimmed shelf (Sopeira and Santa Fe formations, middle Cenomanian to early Turonian) to a flooded platform (Pardina and AguaSalenz Fms, early Turonian to late Coniacian).

The Sopeira MB was controlled by salt-withdrawal (e.g. Gannaway et al., 2022) or by rollover extension in the hangingwall of a buried north dipping listric fault (Gannaway et al., 2022; Saura et al., 2016) geometrically comparable to the Armeña weld. The exposures of the Sopeira MB allow to exhibit stratal pattern evolution and facies distribution from the center part of the MB to the eastern border characterized by N-S trending Llastarri structures interpreted as salt weld (Saura et al., 2016), or faults which bounds remnant buried salt ridge (Gannaway et al., 2022). This exposed section allows to better understand the influence of halokinesis on the stratal pattern and facies distribution in carbonate dominated environments along a subparallel section related to Ribagorçana basin shoreline. Among the main types of halokinetic-induced geometrical relationships observed in the Sopeira MB, Gannaway et al. (2022) have described abrupt stratal thinning (e.g. 354 to 154 m over 1.4 km, and 35 to 0 m over 1.2 km, for the Lower and Middle Aulet Fm respectively) exhibiting internal stratal onlaps and erosional truncation, without evidence for passive diapirism (i.e. halokinetic sequences and reworked salt-diapir detritus). Two types of facies distribution were observed:

(i) for shallow water facies, rapid shallowing eastward trends occurs over distances of ~600m in response to Llastari remnant salt ridge high topography and downbuilding of the Sopeira MB. It is testified by transitions from dominantly upper-shoreface and foreshore facies to upper shoreface and lagoonal facies in the Lower and Middle Aulet Fm. In the Armeña MB, similar shallowing trends impacting inner ramp to outer ramp mixed siliciclastic-carbonate environments over distances <1 km were also observed, but within landward thickening strata (i.e. towards the welded Armeña salt wall, Fig. 12). Compared to the Sopeira MB, this facies distribution suggests that in siliciclastic settings, the primary controls on facies distribution are a seaward main direction of sediment supply combined with local salt-induced depocenters (i.e. landward thickening wedges, Unit 2, Fig. 12) and topographies.

(ii) For deeper water facies, the mixed siliciclastic-carbonate outer-ramp strata of the Cotiella MB involved within the 70° growth strata exhibit very minor lateral facies variation (Unit 3, Fig. 12), suggesting that an elevated salt topography has a minor influence on fine-grained siliciclastic influenced, low-energy, deepwater lithofacies. In the Sopeira MB, lateral variability of deepwater facies is also rare (e.g. Santa Fe, Pardina Fms and the Aguasalenz Fm). However, offshore marine to lower shoreface parasequences constituting the remnant salt-ridge flanking strata of the Upper Aulet Fm in the Sopeira MB, are interstratified with reworked Lower Aulet Fm monolithic blocks previously developed on top of the salt roof (Gannaway et al., 2022). In the Armeña and Cotiella MBs, debrites are absent probably indicating the absence of carbonate platform development on top of the welded Armeña salt wall roof. The relation between the type of sedimentary system and the reworking of diapir roof debrites is discussed below through the comparison with the Bakio diapir flanking strata.

8.2.2 The Bakio Diapir

The Bakio passive diapir is located in the Basque-Cantabrian basin, in the westernmost part of the Pyrenees. The main diapir growth period occurred during the middle Albian involving the formation of composite tapered and tabular halokinetic sequences (Cumberpatch et al., 2020, 2021; Poprawski et al., 2014; Roca et al., 2021), impacting the distribution of carbonate outer-shelf and siliciclastic deepwater facies (García-Mondéjar and Robador, 1987). Wedge-type halokinetic sequences associated with a diapir roof composed of vertically aggrading carbonate platforms exhibit broad zone with some abrupt facies changes and abundant debrites, while the diapir roof with dominantly siliciclastic sediments exhibit broad zone of gradational facies changes with rare debrites (Roca et al., 2021). This difference is related to aggradation of carbonate platforms on top of diapirs in carbonate dominated environments, creating steep slopes on the diapir edges (Poprawski et al., 2016). In the salt-controlled mixed siliciclastic-carbonate sedimentation of the Cotiella MBs, the absence of debrites and abrupt changes of facies along the salt wall implies probably the absence of carbonate platform above the salt wall and/or steep slope on the salt structure edge. This is corroborated by the presence of bi-pyramidal quartz reworked in the flanking salt wall strata, implying indirectly that Keuper evaporites are exposed and not capped during the development of units 2 and 3 (Figs. 11, 12).

9. Conclusion

The Upper Cretaceous post-rift Cotiella Basin exposes exceptionally preserved kilometer thick sedimentary succession of seismic-scale MBs and the salt-structures flanking strata. In order to analyses the impact of a growing salt structure on facies distribution, stratal pattern, and thickness trends, this investigation focuses on the exceptionally preserved syn-halokinetic strata of the Armeña and Cotiella MBs. These latest are bounded by the welded welded Armeña salt wall. Its former existence is borne out by large-scale and small-scale halokinetic folding, growth strata, unconformities, and diapir-derived detritus within the salt-structure flanking strata. To the North, the Armeña MB correspond to extensional rollover MB coeval to salt withdrawal, characterized by a landward-dipping large-scale 80° thickening wedge towards the welded Armeña salt wall. To the South, the Cotiella MB is characterized by an 130° megaflap, exhibiting large-scale thinning wedge and unconformities towards the welded Armeña salt wall.

The syn halokinetic sedimentary infill of the Armeña and Cotiella MBs is characterized by shallow-marine mixed siliciclastic-carbonate sedimentation. Four facies associations were identified and organized vertically as 5 to 30m thick parasequences, evolving from outer ramp fine-grained wackestones (FA1) to middle to inner ramp packstones-grainstones (FA2, FA3) and/or sandy calcarenites (FA4). Based on the regional paleogeography and the local lithofacies trends (i.e. progressive north to northeastward deepening of facies), the shallow-marine sedimentary system is spatially organized along a ~S to N proximal-distal profile. Four depositional sequences were described (S1, S2, S3 and S4) and helped to better expose the timing of salt-induced geometries and depocenters migrations. The tectonostratigraphic evolution of the Cotiella MBs syn-halokinetic strata were subdivided into three main units. The sharp transitions between units are (i) associated with changes in the stratal pattern trends, halokinetic large-scale geometries, stratigraphic thickness trends, the sequence stratigraphic architecture, the sedimentary system as well as the distribution of the facies assemblages, (ii) interpreted as being controlled by halokinetic events, those might be controlled themselves by basin-scale allogenic factors such as tectonic or eustatic factors.

Unit 1 is characterized by the initiation of salt inflation (i.e. salt thickening by internal flow) and salt-extensional rollovers. This phase is associated with carbonate dominated parasequences characterized by

laterally continuous sheet-like layers and progressive facies transitions over distances of kms, despite the ~30% of wedging recorded in the Armeña MB. That suggest that during earliest stage of the rising salt wall, the influence of halokinesis on sedimentation is minor, and only impacts thickness trends and depocenter localization.

The unit 2 is characterized by salt evacuation (i.e. salt extrusion on the seafloor) and rapid downbuilding of the Armeña MB. The stratal pattern is characterized by sheet like layers with shorter progressive facies transitions, over distances of hundreds of meters downdip to the welded Armeña salt wall. Major increase of salt-induced accommodation and wedging rates were recorded in the Cotiella MBs. The sedimentological response is marked by brutal appearance of salt-diapir derived detritus, as well as tide-dominated sandy calcarenites. At a local scale, halokinesis has played an important role in influencing the geometry of the individual sedimentary sequences and the facies distributions, especially along the salt-structure flanking strata. The uncommon E to SE orientation of paleocurrents, indicates a westerly provenance for the clastic material supply suggesting drainage pattern probably primary controlled by salt topographies. This agrees with the direction of the welded Armeña salt wall striking NW-SE, which is compatible with the E to SE paleocurrents. It indicates that the salt evacuation formed topographically elevated salt walls that amplified tidal currents along strike and facilitate the accumulation of sandy-rich facies along the salt wall margin. The analysis of Unit 2 suggests that during the salt evacuation stage of the rising salt wall, the influence of halokinesis on sedimentation is major, as well as its impact on thickness trends and depocenter localization.

Unit 3 records the continuation of the salt evacuation stage and the rapid downbuilding of the Cotiella MB in response to the Armeña MB basal welding. This phase marks a major transition towards fine-grained outer ramp facies involving a brutal decrease of sandy-rich facies ratio, most probably controlled by basin-scale (i.e. tectonic subsidence) or global (i.e. eustatic-driven sea-level rise). The depocenter moved brutally to the South, and a minimum of 1.5km thick sediments were deposited along the northern margin of the Cotiella MB, coeval to the formation of a 70 to 90° large-scale thinning wedge towards the welded Armeña salt wall. All these features suggest that during the end of the salt evacuation stage, the influence of halokinesis on sedimentation is still major, as well as its impact on thickness trends, large-scale geometries and depocenter localization.

Acknowledgements

This research was supported by TotalEnergies as part of the PIT (Projet d'Innovation Technologique) project. The authors would like to thank Jean-Pierre Girard, Jérémie Gaillot, Pierre Masse, Jonathan Pelletier, Jean-Loup Rubino, François Lafont and Jean-Michel Kluska for fruitful discussions. We are also very grateful to Charlie Kergaravat, Vincent Mirande-Rey, Philippe Razin, Nicolas Dall'Asta, Merce Estiarte and Marine Lartigau for their precious help in the field and ensuing discussions. We are also very grateful to reviewers Rachelle Kernen and Mar Moragas for their constructive and helpful comments that helped to improve the manuscript.

Funding

This research was supported by TotalEnergies as part of the PIT (Projet d'Innovation Technologique) Project salt tectonics. We also acknowledge additional support by the research project Structure and Deformation of Salt-bearing Rifted Margins (SABREM), PID2020-117598GB-I00, funded by MCIN/ AEI /10.13039/501100011033.

References

Andrie, J.R., Giles, K.A., Lawton, T.F., Rowan, M.G., 2012. Halokinetic-sequence stratigraphy, fluvial sedimentology and structural geometry of the Eocene Carroza Formation along La Popa salt weld, La Popa Basin, Mexico. Geol. Soc. London, Spec. Publ. 363, 59–79.

Andrieu, S., Saspiturry, N., Lartigau, M., Issautier, B., Angrand, P., Lasseur, E., 2021. Large-scale vertical movements in Cenomanian to Santonian carbonate platform in Iberia: indicators of a Coniacian pre-orogenic compressive stress. BSGF-Earth Sci. Bull. 192, 19.

Aschoff, J.L., Giles, K.A., 2005. Salt diapir-influenced, shallow-marine sediment dispersal patterns: Insights from outcrop analogs. Am. Assoc. Pet. Geol. Bull. 89, 447–469.

Ashley, G.M., 1990. Classification of large-scale subaqueous bedforms; a new look at an old problem. J. Sediment. Res. 60, 160–172.

Banham, S.G., Mountney, N.P., 2013. Evolution of fluvial systems in salt-walled mini-basins: a review and new insights. Sediment. Geol. 296, 142–166.

Barde, J.-P., Chamberlain, P., Galavazi, M., Gralla, P., Harwijanto, J., Marsky, J., van den Belt, F., 2002. Sedimentation during halokinesis: Permo-Triassic reservoirs of the Saigak field, Precaspian basin, Kazakhstan. Pet. Geosci. 8, 177–187.

Boersma, J.R., 1969. Internal structure of some tidal mega-ripples on a shoal in the Westerschelde Estuary, The Netherlands. Geol. en Mijnbouw/Netherlands J. Geosci. 48, 409–414.

Brandano, M., Civitelli, G., 2008. Sequence stratigraphy of the Latium-Abruzzi carbonate ramp (Miocene, Central Apennines, Italy), in: Amorosi, A., Haq, B.U., Sabato, L. (Eds.), Advances in Application of Sequence Stratigraphy in Italy. GeoActa, pp. 217–236.

Brun, J.-P., Fort, X., 2011. Salt tectonics at passive margins: Geology versus models. Mar. Pet. Geol. 28, 1123–1145.

Burchette, T.P., Wright, V.P., 1992. Carbonate ramp depositional systems. Sediment. Geol. 79, 3–57.

Callot, J.-P., Salel, J.-F., Letouzey, J., Daniel, J.-M., Ringenbach, J.-C., 2016. Three-dimensional evolution of salt-controlled minibasins: Interactions, folding, and megaflap development. Am. Assoc. Pet. Geol. Bull. 100, 1419–1442.

Cartigny, M.J.B., Ventra, D., Postma, G., van Den Berg, J.H., 2014. Morphodynamics and sedimentary structures of bedforms under supercritical-flow conditions: new insights from flume experiments. Sedimentology 61, 712–748.

Célini, N., Callot, J.-P., Pichat, A., Legeay, E., Graham, R., Ringenbach, J.-C., 2022. Secondary minibasins in orogens: Examples from the Sivas Basin (Turkey) and the sub-Alpine fold-and-thrust belt (France). J. Struct. Geol. 156, 104555.

Célini, N., Callot, J.-P., Ringenbach, J.-C., Graham, R., 2021. Anatomy and evolution of the Astoin diapiric complex, sub-Alpine fold-and-thrust belt (France). BSGF-Earth Sci. Bull. 192, 29.

Célini, N., Callot, J., Ringenbach, J., Graham, R., 2020. Jurassic salt tectonics in the SW sub-alpine fold-and-thrust belt. Tectonics 39, e2020TC006107.

Civitelli, G., Brandano, M., 2005. Atlante delle litofacies e modello deposizionale dei Calcari a Briozoi e Litotamni nella Piattaforma carbonatica laziale-abruzzese. Bollettino-societa Geol. Ital. 124, 611.

Collie, A.J., Giles, K., 2011. Comparison of Lower Cambrian carbonate facies and halokinetic sequences in minibasins developed on opposite sides of the Wirrealpa Diapir, Central Flinders Ranges, South Australia. in: AAPG annual conference and exhibition, Houston, Texas. 10-13 April.

Csicsek, A., Célini, N., Callot, J.-P., Ringenbach, J.-C., Graham, R., Brooke-Barnett, S., Lonergan, L., 2022. Along-strike variations of salt-related structural style in the Western Alps. in: EGU General Assembly 2022. Copernicus, Vienna, Austria, EGU22-7644. 23-27 May. https://doi.org/10.5194/egusphere-egu22-7644

Cumberpatch, Z., Finch, E., Kane, I., Jackson, C., Hodgson, D., Kilhams, B., Pichel, L., 2020. Halokinetic modulation of sedimentary systems: an integrated approach, in: EGU General Assembly Conference Abstracts., p. 10099, 4-8 May.

Cumberpatch, Z.A., Kane, I.A., Soutter, E.L., Hodgson, D.M., Jackson, C.A.L., Kilhams, B.A., Poprawski, Y., 2021. Interactions between deep-water gravity flows and active salt tectonics. J. Sediment. Res. 91, 34–65.

Dalrymple, R.W., Rhodes, R.N., 1995. Estuarine dunes and bars, in: Perillo, G.M.. (Ed.), Geomorphology and Sedimentology of Estuaries. Elsevier, pp. 359–422.

De Gibert, J.M., Goldring, R., 2007. An ichnofabric approach to the depositional interpretation of the intensely burrowed Bateig Limestone, Miocene, SE Spain. Sediment. Geol. 194, 1–16.

Dietrich, P., Ghienne, J.-F., Normandeau, A., Lajeunesse, P., 2016. Upslope-migrating bedforms in a proglacial sandur delta: Cyclic steps from river-derived underflows? J. Sediment. Res. 86, 112–122.

Dunham, R.J., 1962. Classification of carbonate rocks according to depositional textures, in: Ham, W.E. (Ed.), Classification of Carbonate Rocks. American Association of Petroleum Geologists Memoir, pp. 108–121.

Embry, A.F., Johannesen, E., 1992. T-R sequence stratigraphy, facies analysis and reservoir distribution in the uppermost Triassic-lowermost Jurassic succession, western Sverdrup Basin, Arctic Canada. Norwegian Petroleum Society Special Publications, 121-146.

Fornos, J.J., Ahr, W.M., 1997. Temperate carbonates on a modern, low-energy, isolated ramp; the Balearic Platform, Spain. J. Sediment. Res. 67, 364–373.

Fort, X., Brun, J.-P., Chauvel, F., 2004. Salt tectonics on the Angolan margin, synsedimentary deformation processes. Am. Assoc. Pet. Geol. Bull. 88, 1523–1544.

Fries, G., Parize, O., 2003. Anatomy of ancient passive margin slope systems: Aptian gravity-driven deposition on the Vocontian palaeomargin, western Alps, south-east France. Sedimentology 50, 1231–1270.

Gannaway, C.E., Giles, K.A., Kernen, R.A., Rowan, M.G., Hearon, T.E., 2014. Comparison of suprasalt and subsalt depositional and halokinetic history of Patawarta Diapir, Flinders Ranges, South Australia, in: Pindell, J., Horn, B., Rosen, N., Weimer, P., Dinkleman, M., Lowrie, A., Fillon, R., Granath, J., Kennan, L., (Eds.), Sedimentary Basins: Origin, Depositional Histories, and Petroleum Systems. SEPM, p. 428-429. https://doi.org/10.5724/gcs.14.33.0428

Gannaway, C.E., Giles, K.A., Muñoz, J.A., Rowan, M.G., 2022. Interpreting the nature of the Aulet and Adons diapirs from sedimentologic and stratigraphic analysis of flanking minibasin strata, Spanish Pyrenees, Catalunya, Spain. J. Sediment. Res. 92, 167–209.

García-Mondéjar, J., Robador, A., 1987. Sedimentación y paleografía del Complejo Urgoniano (Aptiense-Albiense) en el área de Bermeo (región Vasco-Cantábrica septentional). Acta geológica hispánica

411–418.

García Senz, J., 2002. Cuencas extensivas del Cretácico Inferior en los Pirineos centrales. Formación y subsecuente inversión. Ph.D. dissertation, Universitat de Barcelona, Barcelona, Spain, p. 310.

Gérard, J.R.F., Bromley, R.G., 2008. Ichnofabrics in clastic sediments: applications to sedimentological core studies: a practical guide. Total-ASF-Repsol, Madrid.

Giles, K.A., Lawton, T.F., 2002. Halokinetic sequence stratigraphy adjacent to the El Papalote diapir, northeastern Mexico. Am. Assoc. Pet. Geol. Bull. 86, 823–840.

Giles, K.A., Rowan, M.G., 2012. Concepts in halokinetic-sequence deformation and stratigraphy. Geol. Soc. London, Spec. Publ. 363, 7–31.

Gómez-Alday, J.J., García-Garmilla, F., Elorza, J., 1994a. Evidencias de actividad diapírica sobre las unidades deposicionales del Maastrichtiense en la zona de Laño. Geogaceta 7, 90–93.

Gómez-Alday, J.J., García Garmilla, F., Elorza, J., 1994b. Caracterización de las Geodas de cuarzo de Lano (sur de Vitoria). Relación con la actividad somerizante del Diapiro de Penacerrada (Cuenca Vasco-Cantábrica). Geogaceta 16, 132–135.

Gräfe, K.U., 2005. Benthic foraminifers and palaeoenvironment in the Lower and Middle Jurassic of the Western Basque-Cantabrian Basin (Northern Spain). J. Iber. Geol. 31, 217–233.

Hallock, P., Hine, A.C., Vargo, G.A., Elrod, J.A., Jaap, W.C., 1988. Platforms of the Nicaraguan Rise: Examples of the sensitivity of carbonate sedimentation to excess trophic resources. Geology 16, 1104–1107.

Haq, B.U., 2014. Cretaceous eustasy revisited. Glob. Planet. Change 113, 44–58.

Haq, B.U., Hardenbol, J., Vail, P.R., 1988. Mesozoic and Cenozoic chronostratigraphy and cycles of sea-level change. Sea-Level Chang. SEPM Spec. Publ. 42, 71–108.

Hartley, A., Evenstar, L., 2018. Fluvial architecture in actively deforming salt basins: Chinle Formation, Paradox Basin, Utah. Basin Res. 30, 148–166.

Hudec, M.R., Jackson, M.P.A., 2007. Terra infirma: Understanding salt tectonics. Earth-Science Rev. 82, 1–28.

Hudec, M.R., Jackson, M.P.A., Vendeville, B.C., Schultz-Ela, D.D., Dooley, T.P., 2011. The salt mine: A digital atlas of salt tectonics, Bureau of Economic Geology, Austin.

Jackson, M.P.A., Hudec, M.R., 2017. Salt tectonics: Principles and practice. Cambridge University Press, Austin.

Jackson, M.P.A., Talbot, C.J., 1986. External shapes, strain rates, and dynamics of salt structures. Geol. Soc. Am. Bull. 97, 305–323.

Jammes, S., Manatschal, G., Lavier, L., Masini, E., 2009. Tectonosedimentary evolution related to extreme crustal thinning ahead of a propagating ocean: Example of the western Pyrenees. Tectonics 28. https://doi.org/10.1029/2008TC002406

Jobe, J.A.T., Giles, K.A., Hearon, T.E., Rowan, M.G., Trudgill, B., Dalton, C.E.G., Jobe, Z.R., 2020. Controls on the structural and stratigraphic evolution of the megaflap-bearing Sinbad Valley salt wall, NE Paradox Basin, SW Colorado. Geosphere 16, 297–328.

Kergaravat, C., Ribes, C., Legeay, E., Callot, J. P., Kavak, K. S., Ringenbach, J. C., 2016. Minibasins and

salt canopy in foreland fold-and-thrust belts: The central Sivas Basin, Turkey. Tectonics 35(6), 1342-1366.

Kergaravat, C., Ribes, C., Callot, J. P., Ringenbach, J. C., 2017. Tectono-stratigraphic evolution of salt-controlled minibasins in a fold and thrust belt, the Oligo-Miocene central Sivas Basin. Journal of Structural Geology 102, 75-97.

Kernen, R.A., Giles, K.A., Rowan, M.G., Lawton, T.F., Hearon, T.E., 2012. Depositional and halokinetic-sequence stratigraphy of the Neoproterozoic Wonoka Formation adjacent to Patawarta allochthonous salt sheet, Central Flinders Ranges, South Australia. Geol. Soc. London, Spec. Publ. 363, 81–105.

Kreisa, D.R., Moila, R.J., 1986. Sigmoidal tidal bundles and other tide-generated sedimentary structures of the Curtis Formation, Utah. Geol. Soc. Am. Bull. 97, 381. https://doi.org/10.1130/0016-7606(1986)

Querol, X., Salas, R., Pardo, G., Ardevol, L., 1992. Albian coal-bearing deposits of the Iberian Range in northeastern Spain. Controls on the distribution and quality of Cretaceous coals. Geol. Soc. America, Spec. Paper 267, 193-208.

Lawton, T.F., Buck, B.J., 2006. Implications of diapir-derived detritus and gypsic paleosols in Lower Triassic strata near the Castle Valley salt wall, Paradox Basin, Utah. Geology 34, 885–888.

Lawton, T.F., Buller, C.D., Parr, T.R., 2015. Provenance of a Permian erg on the western margin of Pangea: Depositional system of the Kungurian (late Leonardian) Castle Valley and White Rim sandstones and subjacent Cutler Group, Paradox Basin, Utah, USA. Geosphere 11, 1475–1506.

Lindholm, R., 2012. A practical approach to sedimentology. Springer Science & Business Media, Winchester.

Lopez-Mir, B., 2013. Extensional salt tectonics in the Cotiella post-rift basin (south-central Pyrenees): 3D structure and evolution. Ph.D. dissertation, Universitat de Barcelona, Barcelona, Spain, p. 302.

Lopez-Mir, B., Muñoz, J.A., García-Senz, J., 2016a. 3D geometric reconstruction of Upper Cretaceous passive diapirs and salt withdrawal basins in the Cotiella Basin (southern Pyrenees). J. Geol. Soc. London. 173, 616–627.

Lopez-Mir, B., Muñoz, J.A., García-Senz, J., 2016b. Geology of the Cotiella thrust sheet, southern Pyrenees (Spain). J. Maps 12, 323–327.

Lopez-Mir, B., Muñoz, J.A., García-Senz, J., 2015. Extensional salt tectonics in the partially inverted Cotiella post-rift basin (south-central Pyrenees): structure and evolution. Int. J. Earth Sci. 104, 419–434.

Macchiavelli, C., Vergés, J., Schettino, A., Fernàndez, M., Turco, E., Casciello, E., Torne, M., Pierantoni, P.P., Tunini, L., 2017. A new southern North Atlantic isochron map: Insights into the drift of the Iberian plate since the Late Cretaceous. J. Geophys. Res. Solid Earth 122, 9603–9626.

Malpas, J.A., Gawthorpe, R.L., Pollard, J.E., Sharp, I.R., 2005. Ichnofabric analysis of the shallow marine Nukhul Formation (Miocene), Suez Rift, Egypt: implications for depositional processes and sequence stratigraphic evolution. Palaeogeogr. Palaeoclimatol. Palaeoecol. 215, 239–264.

Martín-Chivelet, J., Floquet, M., García-Senz, J., Callapez, P.M., López-Mir, B., Muñoz, J.A., Barroso-Barcenilla, F., Segura, M., Soares, A.F., Dinis, P.M., 2019. Late Cretaceous post-rift to convergence in Iberia, in: Quesada, C., Oliveira, J.T. (Eds.), The Geology of Iberia: A Geodynamic Approach. Springer, pp. 285–376.

Masini, E., Manatschal, G., Tugend, J., Mohn, G., Flament, J.-M., 2014. The tectono-sedimentary evolution of a hyper-extended rift basin: the example of the Arzacq–Mauléon rift system (Western Pyrenees, SW France). Int. J. Earth Sci. 103, 1569–1596.

Matthews, W., Hampson, G., Trudgill, B., Underhill, J., 2004. Impact of salt movement on fluvio-lacustrine stratigraphy and facies architecture: Late Triassic Chinle Formation, northern Paradox basin, southeast Utah, USA, in: Post, P.J., Olson, D.L., Lyons, K.T., Palmes, S.L., Harisson, P.F., Rosen, N.C. (Eds.), Salt Sediment Interactions and Hydrocarbon Prospectivity Concepts, Applications and Case Studies for the 21st Century. SEPM, pp. 931–964. https://doi.org/10.5724/gcs.04.24.0931

Matthews, W.J., Hampson, G.J., Trudgill, B.D., Underhill, J.R., 2007. Controls on fluviolacustrine reservoir distribution and architecture in passive salt-diapir provinces: Insights from outcrop analogs. Am. Assoc. Pet. Geol. Bull. 91, 1367–1403.

McClay, K., Muñoz, J.-A., García-Senz, J., 2004. Extensional salt tectonics in a contractional orogen: A newly identified tectonic event in the Spanish Pyrenees. Geology 32, 737–740.

Mey, P.H.W., Nagtegaal, P.J.C., Roberti, K.J., Hartevelt, J.J.A., 1968. Lithostratigraphic subdivision of post-Hercynian deposits in the south-central Pyrenees, Spain. Leidse Geol. Meded. 41, 221–228.

Muñoz, J.A., 1992. Evolution of a continental collision belt: ECORS-Pyrenees crustal balanced cross-section, in: McClay, K.R., (Ed.), Thrust Tectonics. Springer, pp. 235–246.

Pascual-Cebrian, E., 2009. Estratigrafria dels sediments sin-extensius del Coniacià-Santonià del Massís del Cotiella. Mater dissertation, Universitat de Barcelona, Barcelona, Spain, p. 79.

Pichel, L.M., Jackson, C.A., 2020. Four-dimensional variability of composite halokinetic sequences. Basin Res. 32, 1277–1299.

Pomar, L., 2001. Ecological control of sedimentary accommodation: evolution from a carbonate ramp to rimmed shelf, Upper Miocene, Balearic Islands. Palaeogeogr. Palaeoclimatol. Palaeoecol. 175, 249–272.

Pomar, L., Bassant, P., Brandano, M., Ruchonnet, C., Janson, X., 2012. Impact of carbonate producing biota on platform architecture: insights from Miocene examples of the Mediterranean region. Earth-Science Rev. 113, 186–211.

Poprawski, Y., Basile, C., Agirrezabala, L.M., Jaillard, E., Gaudin, M., Jacquin, T., 2014. Sedimentary and structural record of the Albian growth of the Bakio salt diapir (the Basque Country, northern Spain). Basin Res. 26, 746–766.

Poprawski, Y., Basile, C., Jaillard, E., Gaudin, M., Lopez, M., 2016. Halokinetic sequences in carbonate systems: An example from the middle Albian Bakio breccias formation (Basque Country, Spain). Sediment. Geol. 334, 34–52.

Querol, X., Salas, R., Pardo, G., Ardevol, L., 1992. Albian coal-bearing deposits of the Iberian Range in northeastern Spain. Control. Distrib. Qual. Cretac. coals 267, 193–208.

Ribes, C., Kergaravat, C., Bonnel, C., Crumeyrolle, P., Callot, J., Poisson, A., Temiz, H., Ringenbach, J., 2015. Fluvial sedimentation in a salt-controlled mini-basin: stratal patterns and facies assemblages, Sivas Basin, Turkey. Sedimentology 62, 1513–1545.

Ribes, C., Kergaravat, C., Crumeyrolle, P., Lopez, M., Bonnel, C., Poisson, A., Kavak, K.S., Callot, J., Ringenbach, J., 2017. Factors controlling stratal pattern and facies distribution of fluvio-lacustrine sedimentation in the Sivas mini-basins, Oligocene (Turkey). Basin Res. 29, 596–621.

Ribes, C., Lopez, M., Kergaravat, C., Crumeyrolle, P., Poisson, A., Callot, J.-P., Paquette, J.-L., Ringenbach, J.-C., 2018. Facies partitioning and stratal pattern in salt-controlled marine to continental mini-basins: Examples from the Late Oligocene to Early Miocene of the Sivas Basin, Turkey. Mar. Pet. Geol. 93, 468–496.

Roca, E., Ferrer, O., Rowan, M.G., Muñoz, J.A., Butillé, M., Giles, K.A., Arbués, P., de Matteis, M., 2021. Salt tectonics and controls on halokinetic-sequence development of an exposed deepwater diapir: The Bakio Diapir, Basque-Cantabrian Basin, Pyrenees. Mar. Pet. Geol. 123, 104770.

Roca, E., Muñoz, J.A., Ferrer, O., Ellouz, N., 2011. The role of the Bay of Biscay Mesozoic extensional structure in the configuration of the Pyrenean orogen: Constraints from the MARCONI deep seismic reflection survey. Tectonics 30, TC2001. https://doi.org/10.1029/2010TC002735

Rosenbaum, G., Lister, G.S., Duboz, C., 2002. Relative motions of Africa, Iberia and Europe during Alpine orogeny. Tectonophysics 359, 117–129.

Rowan, M.G., Giles, K.A., Hearon IV, T.E., Fiduk, J.C., 2016. Megaflaps adjacent to salt diapirs. Am. Assoc. Pet. Geol. Bull. 100, 1723–1747.

Rowan, M.G., Giles, K.A., Hearon, T.E., Gannaway, C.E., Fiduk, J.C., 2014. Megaflaps along the edges of steep diapirs and beneath salt sheets: Models and examples, in: International Conference & Exhibition. Istanbul, Turkey, 14-17 September.

Rowan, M.G., Lawton, T.F., Giles, K.A., Ratliff, R.A., 2003. Near-salt deformation in La Popa basin, Mexico, and the northern Gulf of Mexico: A general model for passive diapirism. Am. Assoc. Pet. Geol. Bull. 87, 733–756.

Saura, E., Ardèvol i Oró, L., Teixell, A., Vergés, J., 2016. Rising and falling diapirs, shifting depocenters, and flap overturning in the Cretaceous Sopeira and Sant Gervàs subbasins (Ribagorça Basin, southern Pyrenees). Tectonics 35, 638–662.

Sharafi, M., Mahboubi, A., Moussavi-Harami, R., Mosaddegh, H., Gharaie, M.H.M., 2014. Trace fossils analysis of fluvial to open marine transitional sediments: Example from the Upper Devonian (Geirud Formation), Central Alborz, Iran. Palaeoworld 23, 50–68.

Shelley, D.C., Lawton, T.F., 2005. Sequence stratigraphy of tidally influenced deposits in a salt-withdrawal minibasin: Upper sandstone member of the Potrerillos Formation (Paleocene), La Popa basin, Mexico. Am. Assoc. Pet. Geol. Bull. 89, 1157–1179.

Smith, R.I., Hodgson, N., Fulton, M., 1993. Salt control on Triassic reservoir distribution, UKCS central North Sea, in: Geological Society, London, Petroleum Geology Conference Series. Geological Society of London, pp. 547–557.

Souquet, P., 1984. Les cycles majeurs du Crétacé de la paléomarge ibérique dans les Pyrénées Trav. Lab., 47–70.

Souquet, P., 1967. Le Crétacé supérieur sud-pyrénéen en Catalogne, Aragon et Navarre. Ph.D. dissertation, Universite de Toulouse, Toulouse, France, p. 529.

Trudgill, B.D., 2011. Evolution of salt structures in the northern Paradox Basin: Controls on evaporite deposition, salt wall growth and supra-salt stratigraphic architecture. Basin Res. 23, 208–238.

Tugend, J., Manatschal, G., Kusznir, N.J., 2015. Spatial and temporal evolution of hyperextended rift systems: Implication for the nature, kinematics, and timing of the Iberian-European plate boundary. Geology 43, 15–18.

Tugend, J., Manatschal, G., Kusznir, N.J., Masini, E., Mohn, G., Thinon, I., 2014. Formation and deformation of hyperextended rift systems: Insights from rift domain mapping in the Bay of Biscay-Pyrenees. Tectonics 33, 1239–1276.

Vendeville, B.C., Jackson, M., 1991. Deposition, extension, and the shape of downbuilding salt diapirs. in: Annual meeting of the American Association of Petroleum Geologists (AAPG). Dallas, TX (United States), 7-10 Apr.

Visser, M.J., 1980. Neap-spring cycles reflected in Holocene subtidal large-scale bedform deposits: a preliminary note. Geology 8, 543–546.

Yang, C., Nio, S., 1985. The estimation of palaeohydrodynamic processes from subtidal deposits using time series analysis methods. Sedimentology 32, 41–57.

Highlights

- Cotiella Basin exposes exceptionally preserved seismic-scale minibasins and the salt-walls flanking strata
- The Armeña MB correspond to landward-dipping extensional rollover MB coeval to salt withdrawal
- The Cotiella MB is characterized by an 130° megaflap, exhibiting large-scale thinning wedge and unconformities towards the welded Armeña salt wall
- Distinguishing minibasins tectonostratigraphic units is of prime importance
- Tectonostratigraphic units display different archetypal facies distribution, thickness trends and halokinetic structures
- Topographically elevated salt walls amplify tidal currents, implying sandy-rich facies accumulation along the salt wall margin

Declaration of interests

☒ The authors declare that they have no known competing financial interests or personal relationships that could have appeared to influence the work reported in this paper.

☐ The authors declare the following financial interests/personal relationships which may be considered as potential competing interests: